

Radio Sources in Low-Luminosity Active Galactic Nuclei.

IV. Radio Luminosity Function, Importance of Jet Power, and Radio Properties of the Complete Palomar Sample

Neil M. Nagar¹, Heino Falcke², and Andrew S. Wilson³

¹ Kapteyn Institute, Landleven 12, 9747 AD Groningen, The Netherlands
Astronomy Group, Departamento de Física, Universidad de Concepción, Casilla 160-C, Concepción, Chile
e-mail: nagar@astro-udec.cl

² ASTRON, P.O. Box 2, 7990 AA Dwingeloo, The Netherlands
Department of Astronomy, Radboud University Nijmegen, Postbus 9010, 6500 GL Nijmegen, The Netherlands
e-mail: falcke@astron.nl

³ Department of Astronomy, University of Maryland, College Park, MD 20742, U.S.A.
Adjunct Astronomer, Space Telescope Science Institute, 3700 San Martin Drive, Baltimore, MD 21218, U.S.A.
e-mail: wilson@astro.umd.edu

Received 29 October 2004; accepted 05 February 2005

Abstract. We present the completed results of a high resolution radio imaging survey of all (~ 200) low-luminosity active galactic nuclei (LLAGNs) and AGNs in the Palomar Spectroscopic Sample of all (~ 488) bright northern galaxies. The high incidences of pc-scale radio nuclei, with implied brightness temperatures $\gtrsim 10^7$ K, and sub-parsec jets argue for accreting black holes in $\gtrsim 50\%$ of all LINERs and low-luminosity Seyferts; there is no evidence against *all* LLAGNs being mini-AGNs. The detected parsec-scale radio nuclei are preferentially found in massive ellipticals and in type 1 nuclei (i.e. nuclei with broad H α emission). The radio luminosity function (RLF) of Palomar Sample LLAGNs and AGNs extends three orders of magnitude below, and is continuous with, that of ‘classical’ AGNs. We find marginal evidence for a low-luminosity turnover in the RLF; nevertheless LLAGNs are responsible for a significant fraction of present day mass accretion. Adopting a model of a relativistic jet from Falcke & Biermann, we show that the accretion power output in LLAGNs is dominated by the kinetic power in the observed jets rather than the radiated bolometric luminosity. The Palomar LLAGNs and AGNs follow the same scaling between jet kinetic power and narrow line region (NLR) luminosity as the parsec to kilo-parsec jets in powerful radio galaxies. Eddington ratios l_{Edd} ($= L_{\text{Emitted}}/L_{\text{Eddington}}$) of $\leq 10^{-1} - 10^{-5}$ are implied in jet models of the radio emission. We find evidence that, in analogy to Galactic black hole candidates, LINERs are in a ‘low/hard’ state (gas poor nuclei, low Eddington ratio, ability to launch collimated jets) while low-luminosity Seyferts are in a ‘high’ state (gas rich nuclei, higher Eddington ratio, less likely to launch collimated jets). The radio jets are energetically more significant than supernovae in the host galaxies, and are potentially able to deposit sufficient energy into the innermost parsecs to significantly slow the gas supply to the accretion disk.

Key words. accretion, accretion disks — galaxies: active — galaxies: jets — galaxies: nuclei — radio continuum: galaxies — surveys

1. Introduction

1.1. Accretion activity: Ubiquity and Scaling

It is now clear that there is no sharp division between “active” galactic nuclei (AGN; i.e. nuclei presumably powered by accretion onto a nuclear supermassive [$\gg 10^5 M_{\odot}$] black hole) and “inactive” or “normal” galactic nuclei (nuclei powered by star-formation-related processes). Rather, there is a continuous sequence of activity levels

between these two extremes. There are two lines of evidence for this continuity. The first comprises the ubiquity of black holes and the correlations between black hole mass, galaxy bulge mass and galaxy bulge velocity dispersion (Richstone et al., 1998; Ferrarese & Merritt, 2000; Gebhardt et al., 2000; Merritt & Ferrarese, 2001; Tremaine et al., 2002; Marconi & Hunt, 2003). These results support the idea that many galactic nuclei are quasar relics (Soltan, 1982) and highlight the importance of studying the coeval evolution of a galaxy and its nuclear black hole. The second line of evidence is that

many nearby galaxy nuclei not considered to be powerful AGNs, show several characteristics in common with powerful AGNs. These similarities include the presence of compact radio nuclei and sub-parsec to 100 pc-scale radio jets (e.g. Heckman, 1980; Nagar et al., 2002a), emission line ratios characteristic of powerful AGNs (e.g. Heckman, 1980; Ho et al., 1997a), broad $H\alpha$ lines (Ho et al., 1997b), broader $H\alpha$ lines in polarized emission than in total emission (Barth et al., 1999), water vapor megamasers (Braatz et al., 1997), and nuclear point-like UV sources (Maoz et al., 1995; Barth et al., 1998).

Important results on the growth of galaxies and their black holes, and on the properties and history of accretion in AGNs, are now being provided by several large surveys, e.g. the Sloan Digital Sky Survey (SDSS; Stoughton et al., 2002). An important complement to these large (and higher redshift) surveys of AGNs is the study of so-called low-luminosity AGNs (LLAGNs; i.e. low-luminosity Seyferts, LINERs, and “transition” nuclei [nuclei with spectra intermediate between those of LINERs and H II regions]). Here we use the term LLAGN in a more agnostic manner than AGN: we assume that AGNs are powered by accretion onto a supermassive black hole but make no *a priori* assumption about the power source of LLAGNs. The emission-line luminosities of LLAGNs ($L_{H\alpha} \leq 10^{40}$ erg s $^{-1}$ by definition; Ho et al., 1997a) are a factor $\sim 10^2$ times weaker than typical SDSS AGNs. If LLAGNs are truly (weak) AGNs, then extending our studies to LLAGNs is important as they greatly outnumber powerful AGNs. LLAGNs are best studied in close ($\lesssim 30$ Mpc) nuclei, as a result of sensitivity limitations and the need to attain adequate linear resolution to separate any weak accretion related emission from that of the bright host galaxy. In this paper we focus on the radio properties of the ~ 200 LLAGNs and AGNs (median distance ~ 17 Mpc) in the Palomar spectroscopic sample of ~ 488 bright northern galaxies (Ho et al., 1997a). The weak emission-lines of the Palomar LLAGNs can be modeled in terms of photoionization by hot, young stars (Terlevich & Melnick, 1985; Filippenko & Terlevich, 1992; Shields, 1992), by collisional ionization in shocks (Koski & Osterbrock, 1976; Fosbury et al., 1978; Heckman, 1980; Dopita & Sutherland, 1995) or by starbursts (Alonso-Herrero et al., 1999). Alternatively, they could trace AGNs accreting either at very low accretion rates (with radiated luminosity as low as $\sim 10^{-2} - 10^{-7}$ of the Eddington Luminosity, $L_{\text{Eddington}}$), or at radiative efficiencies (the ratio of radiated energy to accreted mass) much lower than the typical value of $\sim 10\%$ (e.g. Chapter 7.8 of Frank, King, & Raine, 1995) assumed for powerful AGNs.

Closely related to these theoretical and observational studies of the radiation from LLAGNs is the increasing number of accurate mass determinations for “massive dark objects”, presumably black holes, in nearby galactic nuclei, as measured directly by kinematics (e.g. Gebhardt et al., 2003) or inferred via the correlation between black hole mass (M_{BH}) and central

stellar velocity dispersion (σ_c ; Ferrarese & Merritt, 2000; Gebhardt et al., 2000; Merritt & Ferrarese, 2001; Tremaine et al., 2002) or galaxy bulge mass (Richstone et al., 1998; Marconi & Hunt, 2003). These mass determinations, coupled with the emitted luminosity from the AGN, enable a measure of the Eddington ratio, i.e. the emitted accretion luminosity in units of the Eddington luminosity ($l_{\text{Edd}} = L_{\text{Emitted}}/L_{\text{Eddington}}$). In this paper we argue that accounting for the kinetic power in the radio jet is crucial when estimating L_{Emitted} (and hence l_{Edd}) in LLAGNs even though the radiated luminosity in the radio band is bolometrically unimportant. Our high resolution radio observations of a large number of nearby LLAGNs considerably increase the number of LLAGNs with reliable black hole mass estimates *and* high resolution radio observations, allowing a better test of the relationship between these quantities.

1.2. Identifying weak AGNs via their Radio Emission

As discussed in Sect. 1 of Nagar et al. (2002a), a sub-parsec, high brightness temperature ($T_b \gtrsim 10^7$ K), flat spectrum nuclear radio source and any radio jets are reliable indicators of the presence of an accreting supermassive black hole. Interestingly, compact flat spectrum radio nuclei are also detected toward the ~ 10 - $15 M_{\odot}$ black holes in Galactic X-ray binary sources, especially during phases of highly sub-Eddington accretion (see review by Fender & Belloni, 2004). The only known sources of $\log [T_b \text{ (K)}] \geq 5$ radio emission in compact starbursts are radio supernovae (RSNe) within the starburst (e.g. Condon et al., 1991; Smith et al., 1998). However, even RSNe or groups of RSNe cannot reproduce the compactness, high brightness temperatures, and flat spectral indices seen in the radio nuclei of LLAGNs (discussed in Sect. 6). It then only remains to use the radio morphology and spectral shape to test whether the radio emission originates from a jet (possibly relativistic) launched by the black hole or from the accretion flow itself. Radio emission is expected from radiatively inefficient accretion flows (RIAFs), e.g. advection-dominated (ADAF; Narayan et al., 1998) or convection-dominated (CDAF; Narayan et al., 2000) accretion flows, possible forms of accretion onto a black hole at low accretion rates (Rees et al., 1982).

We have argued (Nagar et al., 2002a) that the combination of the Very Large Array¹ (VLA; Thompson et al., 1980) and the Very Long Baseline Array¹ (VLBA; Napier et al., 1994) makes a highly effective and efficient tool to unambiguously identify weak AGNs in bright galactic nuclei. The main advantages are the minimal obscuration at high gigahertz frequencies, the high resolution which allows one to easily pick out the AGN as most radio

¹ The VLA and VLBA are operated by the National Radio Astronomy Observatory, a facility of the National Science Foundation operated under cooperative agreement by Associated Universities, Inc.

emission from other sources is usually resolved out, and the high sensitivity.

1.3. Previous and Future Work in this Series

The effectiveness of radio searches for AGNs in LLAGNs is borne out by the results of previous papers in this series. These include results of VLA and VLBA observations of 48 LINERs (Nagar et al., 2000; Falcke et al., 2000, Papers I and II), and a distance-limited ($D \leq 19$ Mpc) sample of 96 LLAGNs (Nagar et al., 2002a, Paper III), from the Palomar Sample. These papers showed that $\gtrsim 50\%$ of all LINERs and low-luminosity Seyferts have compact flat-spectrum radio nuclei at 150 mas resolution. Follow-up VLBA imaging attained a 100% detection rate of high brightness temperature milli-arcsec scale nuclei in a radio-flux limited subsample. The compactness, high brightness-temperature ($\geq 10^6$ K), and other properties, all argue for an origin of the radio emission in AGN-related processes. The morphology (sub-parsec jets are detected in several nuclei) and radio spectral shape (Nagar et al., 2001, 2002b) support the dominant source of radio emission as the self-absorbed base of a relativistic jet launched by the black hole, rather than a radiatively inefficient accretion inflow. Compact radio nuclei are preferentially found in massive ellipticals and in type 1 nuclei. The core radio luminosity is correlated with the nuclear optical ‘broad’ $H\alpha$ luminosity, the nuclear optical ‘narrow’ emission-line luminosity and width, and the galaxy luminosity (Nagar et al., 2002a). In these correlations, LLAGNs fall close to the low-luminosity extrapolations of more powerful AGNs. The sub-arcsec radio luminosity is correlated with both the estimated mass of the nuclear black hole and the galaxy bulge luminosity. Partial correlation analysis on the two correlations yields the result that each correlation is meaningful even after removing the effect of the other correlation (Nagar et al., 2002a).

This paper presents completed results of our high resolution radio imaging survey of all LLAGNs and AGNs in the Palomar Sample. Future papers will present results on the 1.4 GHz to 667 GHz radio spectral shapes of a subsample of LLAGNs (Nagar et al., in prep; preliminary results in Nagar et al., 2002b) and the sub-pc jet morphology and jet proper motions in LLAGNs (Nagar et al., in prep).

1.4. Organization of this Paper

In the following sections, we first define the sample used (Sect. 2) and then summarize previous observations and report on new VLA and VLBA observations which complete the radio survey of LLAGNs and AGNs in the Palomar sample (Sect. 3). The results of all the VLA and VLBA radio observations of the Palomar sample are presented in Sect. 4. These results are used to synthesize an overall picture of the incidence and properties of

AGNs in LLAGNs – including the radio luminosity function, importance of jet energetics, and correlations with other emission-line and host galaxy properties – and their continuity with more powerful AGNs (Sect 5). The results are briefly discussed in Sect. 6 and the major conclusions of the completed radio study are listed in Sect. 7. Finally, the appendix contains a compilation of high resolution radio observations of the 53 absorption-line nuclei in the Palomar sample. In this paper, as in previous papers of this series, we use a Hubble constant $H_0 = 75 \text{ km s}^{-1} \text{ Mpc}^{-1}$ to be consistent with Ho et al. (1997a) who tabulate the results of optical spectroscopy of the Palomar sample. In this paper we use ‘radio luminosity’ to denote the radiated power at a given radio frequency and ‘jet power’ or ‘jet kinetic power’ to denote the kinetic or mechanical power in the jet (as derived from models of relativistic jets).

2. Sample

The results in this paper, and the new observations reported here, are based on LLAGNs and AGNs selected from the Palomar spectroscopic survey of all (~ 488) northern galaxies with $B_T < 12.5$ mag (Ho et al., 1995). Spectroscopic parameters (including activity classification) of 418 galaxies in the Palomar spectroscopic survey which show nuclear emission lines have been presented in Ho et al. (1997a); updates to these, and upper limits to the emission-line fluxes of a further 53 nuclei without detected emission-lines, are presented in Ho, Filippenko, & Sargent (2003a). Of the 418 galaxies with nuclear emission lines in Ho et al. (1997a), we consider only the 403 which belong to the defined Palomar sample. We thus included in our radio survey approximately 7 AGNs and 190 LLAGNs (using the operational boundary of $L_{H\alpha} \leq 10^{40} \text{ erg s}^{-1}$ to distinguish LLAGNs from AGNs: Ho et al. 1997a). The 206 nuclei with HII region type spectra which make up the balance of the 403 are excluded from our survey. Of the 7 AGNs, only two (NGC 1275 and NGC 4151) have $H\alpha$ luminosities significantly greater than the boundary between AGNs and LLAGNs. The other five AGNs are within a factor ~ 2 of the boundary. In view of the significant photometric uncertainties (for some of these nuclei) and the large aperture of the $H\alpha$ luminosity measurements, these 5 AGNs could be loosely considered as LLAGNs. Thus, while we use ‘Palomar LLAGNs and AGNs’ to describe the sample observed in the radio, it is worth bearing in mind that this sample is almost exclusively comprised of LLAGNs. We have not observed the 53 nuclei without detected emission lines (Ho, Filippenko, & Sargent, 2003a), but list their radio flux densities, derived from the literature, in the Appendix.

3. Radio Observations of the Palomar Sample

Several earlier surveys have targeted a substantial fraction of the nearby galaxies which are now in

the Palomar Sample. Radio surveys with resolution $\sim 1''$ – $10''$ include those by Heckman, Crane, & Balick (1980); Hummel (1980); Wrobel & Heeschen (1984); Hummel et al. (1987); Fabbiano, Gioia & Trinchieri (1989); Carral, Turner, & Ho (1990); Wrobel & Heeschen (1991); Laurent-Muehleisen et al. (1997) and Wrobel et al. (2004). Higher resolution surveys (VLBA or VLBI) include those by Jones, Terzian, & Sramek (1981) and Hummel et al. (1982).

Since the publishing of comprehensive optical results on the Palomar Sample, three groups have conducted large radio surveys of the sample. Our group has now completed a $0''.15$ resolution 15 GHz (2 cm) VLA survey of all LLAGNs except some transition nuclei at $D > 19$ Mpc (a total of 162 nuclei observed; Nagar et al., 2000, 2002a, this work). We then observed all strong sources with the VLBA unless they had already been observed at VLBI resolution (Falcke et al., 2000; Nagar et al., 2002a, this work). Ho & Ulvestad (2001) and Ulvestad & Ho (2001a) have observed all (45) Palomar Seyferts at arcsec resolution at 5 GHz (6 cm) and 1.4 GHz (20 cm) and followed up the strong detections at multiple frequencies with the VLBA (Anderson, Ulvestad, & Ho, 2004). Filho et al. (2000) and Filho et al. (2004) have completed a $5''$ – $0''.3$ resolution survey of all transition nuclei in the sample with follow up VLBA observations of some of the stronger nuclei. Finally, Ulvestad & Ho (2001b) have completed a survey of a well-defined sub-sample of 40 HII type nuclei in the Palomar sample and found that none of them has a compact radio nucleus at the flux levels of those in LLAGNs in the sample. The latter result justifies the exclusion of HII type nuclei from the remaining discussion of this paper.

With the new VLA observations reported here, all except 4 of the LLAGNs and AGNs in the Palomar sample have now been observed at sub-arcsec resolution with the VLA. The four exceptions are: NGC 5850, NGC 5970, NGC 5982, and NGC 5985. We believe that none of these four nuclei would have been detected in our survey, since their measured fluxes are < 1 mJy in observations at 1.4–5 GHz with $1''$ – $5''$ resolution (Hummel et al., 1987; Wrobel & Heeschen, 1991). With the new VLBA observations reported here, all Palomar LLAGNs and AGNs with $S_{15\text{ GHz}}^{\text{VLA}} > 2.7$ mJy (except NGC 5377) have been observed at milli-arcsecond resolution with the VLBA.

3.1. New VLA Observations and Data Reduction

Fifty one Seyferts and LINERs at $D > 19$ Mpc were observed at 15 GHz (2 cm) with the VLA in a 14 hr run on 2001 January 13 and 14. The VLA was in A-configuration (Thompson et al., 1980) at this time and was configured to observe in full polarization mode with two channels (“IF”s) of 50 MHz each. Most target sources were observed at elevations between 40° and 60° ; only a few southern sources were observed at lower elevations, but always above 33° . Each target source was observed with a 7 min integration sandwiched between two 1 min observations

on a nearby strong point-like source (the ‘phase calibrator’). Typically, each target galaxy was observed once in this way; for a handful of galaxies, we were able to make two such passes. The following galaxies not in the Palomar sample, but selected for having accurate black hole mass measurements (Richstone et al., 1998), were also observed during the run: NGC 205, NGC 221, NGC 821, NGC 1023, NGC 2300, NGC 7332, NGC 7457, and NGC 7768.

Data were calibrated and mapped using AIPS, following the standard reduction procedures as outlined in the AIPS cookbook². Elevation dependent effects were removed using the post-October 2000 antenna gain solutions, along with corrections for the sky opacity during the run. Observations of 3C 286 (observed at elevation 50°) were used to set the flux-density scale at 15 GHz. A second flux calibrator, 0410+769 (a.k.a. 0409+768; observed at elevation 47°), was also observed as a flux check source. The 1σ error in flux bootstrapping (i.e. setting the flux density scale relative to the flux calibrators) is expected to be roughly 2.5%.

Maps in Stokes I were made with task IMAGR. Since most targets were observed in ‘snapshot mode’ (i.e. for a short period at a single hour angle), the synthesized beam was not optimal, some of the maps have a low signal-to-noise ratio and any extended structure would not have been mapped properly. For sources stronger than about 3 mJy, we were able to iteratively self-calibrate the data so as to increase the signal-to-noise ratio in the final map. The total flux of the source did not change appreciably during this self calibration process; we therefore did not scale up (to compensate for errors in the phase calibration process) the fluxes of sources weaker than 3 mJy. The resolution of the final maps was $\sim 0''.15$. The typical root mean square (r.m.s.) noise in the final maps was 0.3 mJy and we use a formal detection limit of 1.5 mJy (i.e. 5σ). However, weaker sources (down to 0.7 mJy) have been tentatively detected in some nuclei with positions coincident with the highly accurate positions of the optical nuclei (Cotton, Condon, & Arbizzani 1999).

3.2. New VLBA Observations and Data Reduction

In order to obtain uniform mas-resolution maps of *all* LLAGNs and AGNs in the Palomar sample with $S_{15\text{ GHz}}^{\text{VLA}} > 2.7$ mJy, we selected 10 LLAGNs from Table 1 which had not previously been observed at high enough resolution, signal-to-noise, or image fidelity with the VLBA or VLBI at 5 GHz. These ten LLAGNs, plus one galaxy with an HII type nucleus (NGC 3690), were observed with the VLBA at 4.9 GHz (6 cm) in a 15 hour run on December 17, 2001.

All observations were performed in single polarization (‘LL’) mode, with 128 Megabits per second bitrate, and with 4 channels (“BB”s) of bandwidth 8 MHz each. Each source was observed at two or three different hour angles in order to obtain good (u, v)-coverage. For each source,

² available online at www.nrao.edu

the first observation pass used a cycle of 4 min on source and 1 min on a nearby (distance 1.5° – 5.5°) phase calibrator, repeated seven times. The second pass used a cycle of 2 min on source and 1 min on a nearby phase calibrator, repeated 13 times. The total integration time on each source was therefore at least (and typically) 54 min. The “fringe finder” sources J0555+3948 and J0927+3902 were briefly observed and later used for first order synchronization of the data from the different antennas. The weather was mostly fair at all VLBA sites. There were a few intermittent tape problems at several antennas; all data points with tape weights less than 0.7 (on a scale of 0 to 1) were deleted. Data were calibrated using AIPS, closely following the procedures in the ‘VLBA pipeline’ (Sjouwerman et al., in prep). Bad (u, v) data were deleted before the phase solutions of the phase-calibrator observations were transferred to the galaxy data.

Images in Stokes I (assuming no circular polarization) of the sources were made using AIPS task IMAGR. For sources stronger than about 3 mJy, we were able to iteratively self-calibrate and image the data so as to increase the signal-to-noise in the final map. The peak flux-density of the source typically increased by a factor of 1.3 during the self-calibration process. Therefore, for sources weaker than 4 mJy, on which accurate self-calibration was not possible, we have multiplied the *peak* detected flux-density by 1.3 as a crude attempt to correct for atmospheric decorrelation losses. The r.m.s. noise in the final, uniformly-weighted images is typically 0.15 mJy to 0.2 mJy, and the resolution between 2 mas and 5 mas.

4. Results of the Radio Observations

4.1. Results of the VLA Observations

The detection rate of radio nuclei with the VLA is illustrated in Fig. 1. When all LLAGNs and AGNs in the Palomar sample are considered, the VLA observations have detected 21 of 45 ($47\% \pm 10\%$) Seyferts, 37 of 84 ($44\% \pm 7\%$) LINERs, and 10 of 64 ($16\% \pm 5\%$) transition nuclei, at a resolution of $\sim 0''.15$ and above a flux limit of 1–1.5 mJy. Additionally, one H II type nuclei (NGC 3690) was also detected. Alternatively, one can state that radio nuclei with luminosity $L_{15\text{ GHz}}^{\text{core}} \geq 10^{20} \text{ W Hz}^{-1}$ are found in 15 of 45 Seyferts, 27 of 84 LINERs, and 6 of 64 transition nuclei. The radio luminosities of the detected 15 GHz nuclei lie between 10^{18} and $10^{23} \text{ W Hz}^{-1}$, similar to the luminosities seen in ‘normal’ E/S0 galaxies (Sadler et al., 1989). It is notable, however, that a significant fraction of the detected 15 GHz compact nuclei are in spiral galaxies. Most of the detected 15 GHz nuclear radio sources are compact at the $0''.15$ resolution (typically 15–25 pc) of our survey; the implied brightness temperatures are typically $T_b \geq 10^{2.5-4.0} \text{ K}$.

A complete list of results of the VLA observations of all Palomar LLAGNs and AGNs appears in Table 1 with columns explained in the footnotes. All table columns are listed for sources observed by us; for data taken from the

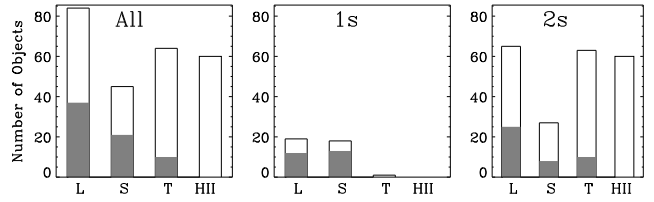


Fig. 1. Detection rate of 15 GHz 150-mas-scale radio nuclei for “L”INERs, “S”eyferts, and “T”ransition nuclei in the Palomar sample. The total number of objects is shown by the upper histogram and the number detected is shown by the grey-shaded histogram. Note the higher detection rates of type 1 (i.e. galaxies with broad H α emission) Seyfert and LINER nuclei.

literature we list only the peak and total flux, the peak luminosity and the reference in which these and the remaining data of the table can be found. For the new VLA observations reported here (Sect. 3.1) the radio positions of detected nuclei were measured directly in J2000 coordinates. For detections reported earlier in Nagar et al. (2000) and Nagar et al. (2002a), we have precessed the B1950 coordinates reported there to equinox J2000 using the SCHED software (the software used to create VLBA observing scripts). The radio positions for the detected nuclei are limited by the positional accuracy of the phase calibrators (typically 2–10 mas), and by the accuracy of the Gaussian fit to the source brightness distribution, which depends on the signal-to-noise ratio of the source detection. The overall accuracy should typically be better than ~ 50 mas. We have compared the radio positions derived here with optical positions from Cotton et al. (1999a), which were measured from the digital sky survey with typical 1σ accuracy $1''.5$ – $2''.5$ in each of right ascension and declination. The results (col. 7 of Table 1) show a good ($\leq 2\sigma$) agreement in most cases. Very few nuclei show reliable extended structure in our 15 GHz maps; the absence of extended emission in most nuclei is not surprising as the high resolution may resolve it out. In addition, such extended emission is expected to be weak at the high frequency observed.

For all the 8 additional sources (i.e. not in the Palomar sample) with accurate black hole masses and observed in the January 2001 VLA run (Sect. 3.1), we can place firm 5σ upperlimits of 1.5 mJy on the nuclear radio emission.

4.2. Results of the VLBA or VLBI Observations

All ten LLAGNs newly observed with the VLBA at 5 GHz were clearly detected in initial maps (i.e. without any form of self-calibration). The single H II type nucleus observed, NGC 3690, was not detected in our observations; a weak (1.5 mJy) high brightness-temperature ($> 10^7 \text{ K}$) radio nucleus in this source was detected in previous deep 1.4 GHz VLBI observations (Lonsdale, Smith, & Lonsdale, 1993). Of the nuclei detected in our observations, mas-scale radio cores were

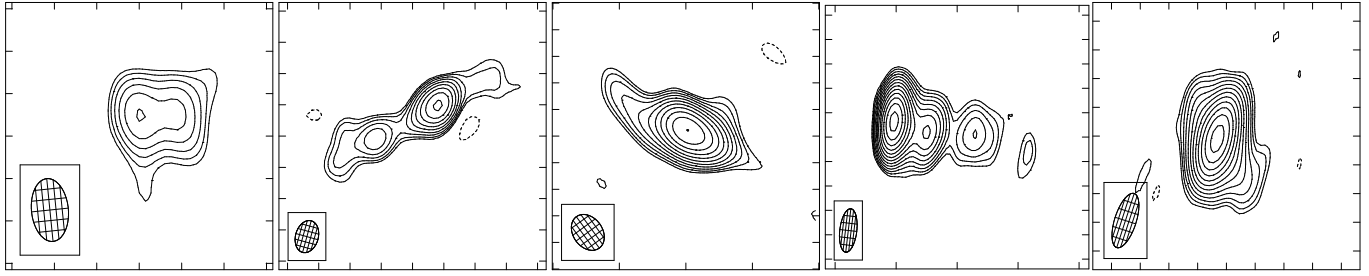


Fig. 2. 5 GHz (6 cm) VLBA maps of (left to right) NGC 2273, NGC 4589, NGC 5353, NGC 5363, and NGC 7626. The contours are integer powers of $\sqrt{2}$, multiplied by the 2σ noise level of 0.25 mJy (0.3 mJy in the case of NGC 5353). The peak flux-densities are 20.6, 6.1, 13.7, 26.1, and 19.0 mJy/beam, respectively. Tick marks are every 2 mas except for NGC 5353 and NGC 5363 (5 mas).

already known to exist in NGC 1167 (Sanghera et al., 1995; Giovannini et al., 2001), NGC 2911 (Schilizzi et al., 1983; Slee et al., 1994; Filho, Barthel, & Ho, 2002), NGC 5353, NGC 5363 (Hummel et al., 1982), and NGC 7626 (Xu et al., 2000). Additionally, NGC 2273 (Lonsdale, Lonsdale, & Smith, 1992) was also suspected of having a mas-scale radio core. Contour maps of the sources found to be extended in our new VLBA observations are shown in Fig. 2. Images of the other radio nuclei with extended mas-scale structure can be found in Falcke et al. (2000), Nagar et al. (2002a, and references therein), Anderson, Ulvestad, & Ho (2004), and Filho et al. (2004).

The VLBA observations confirm that all except one (NGC 2655) nucleus with $S_{\text{VLA}}^{15\text{GHz}} > 2.7$ mJy are genuine AGNs with the radio emission coming from mas- or sub-parsec-scales. A compilation of the results of all VLBA and VLBI observations of LLAGNs and AGNs in the Palomar sample is presented in Table 2, with columns explained in the footnotes. Of the 44 sources listed in the table, 39 are from the flux-limited sample (i.e. $S_{\text{VLA}}^{15\text{GHz}} > 2.7$ mJy in Table 1). Radio positions of sources with data taken from the literature can be found in the references listed in col. 18. For sources from this and our previous works we list source positions referenced to the positions of their respective phase-calibrators. All of these source positions have been updated to reflect the latest (as of January 2004) phase calibrator positions (expected accuracy ~ 1 mas; Beasley et al., 2002). The other factors contributing to the position uncertainty are the accuracy of the Gaussian fit to the target source - which should typically be better than 2 mas - and the error in transferring the phase-calibrator position to the source - which is expected to be better than 3 mas given the small angular separations between our source-phase-calibrator pairs (see e.g. Fig. 3 of Chatterjee et al., 2004). Thus the overall accuracy of the positions listed in Table 2 should be better than 5 mas. The implied brightness temperatures were calculated using the formula given in Falcke et al. (2000); the results are in the range $> 10^{6.3}\text{K}$ to $\gtrsim 10^{10.8}\text{K}$. Since most of the sources are unresolved, these values are lower limits to the true brightness temperatures.

It is interesting to note that the VLBI-detected nuclei in Table 2 include two galaxy pairs in which both members of the pair host an AGN. NGC 3226 and NGC 3227 (which together form Arp 94) are a galaxy pair (internuclear distance $\sim 2.2'$ or ~ 13 kpc) in a strong encounter with prominent tidal plumes. NGC 5353 and NGC 5354 have a nuclear separation of $\sim 1.2'$ or ~ 12 kpc, and are members of Hickson compact group 68 (HCG 68).

5. Radio Properties

5.1. Correlations between Radio Luminosity, Optical Emission-Line and Host Galaxy Properties

Correlations between radio, optical emission line, and host galaxy properties in the Palomar Sample have been addressed in detail for all Seyferts (Ulvestad & Ho, 2001a), all (96) LLAGNs at $D \leq 19$ Mpc (Nagar et al., 2002a), and all transition nuclei (Filho et al., 2004). The results from these papers are essentially unchanged after expanding the sample to include all LLAGNs and AGNs in the Palomar sample. Here we present only an update on the relation between radio luminosity and optical emission-line luminosity (Fig. 3). The elliptical radio detections (filled symbols in the left panel) are closely related to FR Is, as found earlier by Nagar et al. (2002a). The late-type Palomar Seyferts detected in the radio (filled triangles in the right panel) on the other hand lie closer to the region (and its low luminosity extrapolation) occupied by ‘classical’ Seyferts (see also Nagar et al., 2002a).

5.2. Radio Luminosity and Black Hole Mass

Correlations between radio luminosity, black hole mass, and galaxy luminosity have been discussed in Nagar et al. (2002a) using all of the 150 mas resolution VLA radio data listed in this paper along with sub-arcsecond resolution radio data on other nearby galaxies with black hole mass (M_{BH}) estimates. Nagar et al. (2002a) found that the radio luminosity is correlated with both the black hole mass and the bulge luminosity at the 99.99% significance level. Partial correlation analysis on the two correlations yielded the result that each correlation is mean-

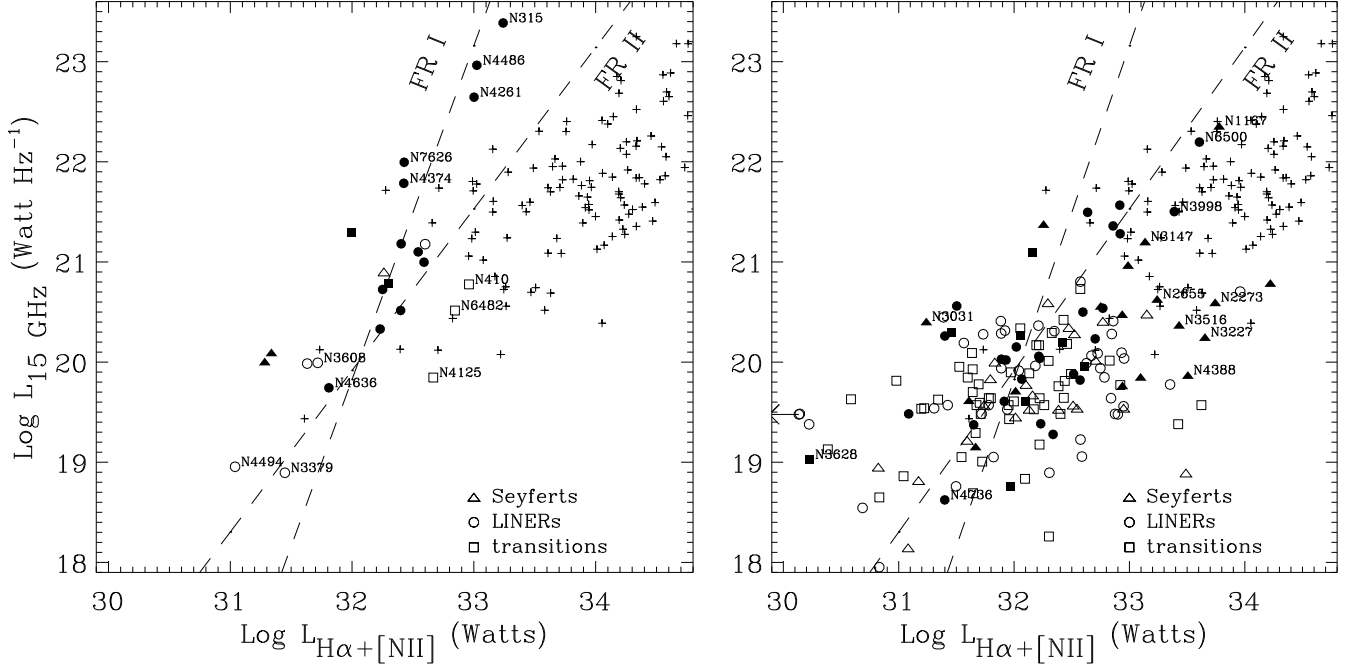


Fig. 3. A plot of the log of the 15 GHz nuclear (150 mas resolution) radio luminosity versus nuclear $H\alpha+[N II] \lambda\lambda 6548, 6583$ luminosity for all LLAGNs and AGNs in the Palomar sample in elliptical (left) and non-elliptical (right) host galaxies. In both panels, Seyferts, LINERs, and transition nuclei from the Palomar sample are shown as triangles, circles, and squares, respectively. For these, filled symbols are used for radio detected nuclei and open symbols are used for upper limits to the radio luminosity. For comparison, radio-detected “classical” Seyfert galaxies (from Whittle 1992a, i.e. not from the Palomar Sample) are plotted as crosses in both panels, regardless of their galaxy morphological type (for these the $[O III]$ luminosity was converted to an $H\alpha+[N II]$ luminosity using standard flux ratios for Seyferts; see Nagar et al. 2002a). Also shown are the low-luminosity extrapolations of linear fits to the same relationship for FR I and FR II radio galaxies (dashed lines; Zirbel & Baum, 1995).

ingful even after removing the effect of the other correlation. Since then a ‘fundamental plane’ between black hole mass, X-ray luminosity, and radio luminosity, which fits both Galactic black hole candidates and AGNs has been claimed by Merloni, Heinz, & di Matteo (2003) and Falcke, Kording, & Markoff (2004).

Here we refine the correlations presented in Nagar et al. (2002a) by considering only nuclei observed with linear resolution ≤ 1 pc in the radio and for which one radio component can be relatively unambiguously identified with the location of the central engine. This resolution and morphological criterion enables a more accurate measure of the radio emission from only the accretion inflow and/or the sub-parsec base of the jet, and helps avoid contamination from radio emission originating in knots further out in the jet. The latter radio emission is common in LLAGNs (Sect. 5.4) and often dominates the parsec scale radio emission in Seyferts. In fact many Seyferts have several radio sources in the inner parsec, none of which are unambiguously identifiable with the central engine (Kukula et al., 1999; Mundell et al., 2003; Middelberg et al., 2004).

Fig. 4 shows the relation between sub-parsec radio luminosity, M_{BH} , and host galaxy bulge luminosity in the B-

band. Black hole masses are either directly measured from stellar, gas, or maser dynamics, or estimated from the central stellar velocity dispersion, σ_c (Emsellem et al., 1999; Gebhardt et al., 2003, for all other references see Nagar et al. 2002a). We used the relationship of Tremaine et al. (2002) to estimate M_{BH} from σ_c . For the circles and triangles in the plot, we also show the error in the black hole mass determination (Fig. 4a). These errors represent reported 1σ errors for masses measured directly from stellar, gas, or maser dynamics (e.g. Gebhardt et al., 2003), or reflect 1σ errors in the reported central stellar velocity dispersion (σ_c) assuming no additional error in converting σ_c to black hole mass (Tremaine et al., 2002).

The plotted circles show the 44 galaxies in Table 2, except NGC 266 (linear resolution 1.3 pc; plotted as a cross), NGC 1167, NGC 4772 (no measurement of σ_c in the literature), and NGC 2655 (not detected with the VLBA). NGC 4395 (in the Palomar sample, and detected in deep VLBA observations; Wrobel, Fassnacht, & Ho, 2001) is taken to not have a bulge (Filippenko & Ho, 2003). In addition, we plot (as triangles) 6 galaxies which are not Palomar LLAGNs or Palomar AGNs and which have radio nuclei relatively unambiguously identified with the central engine in maps with resolution better than

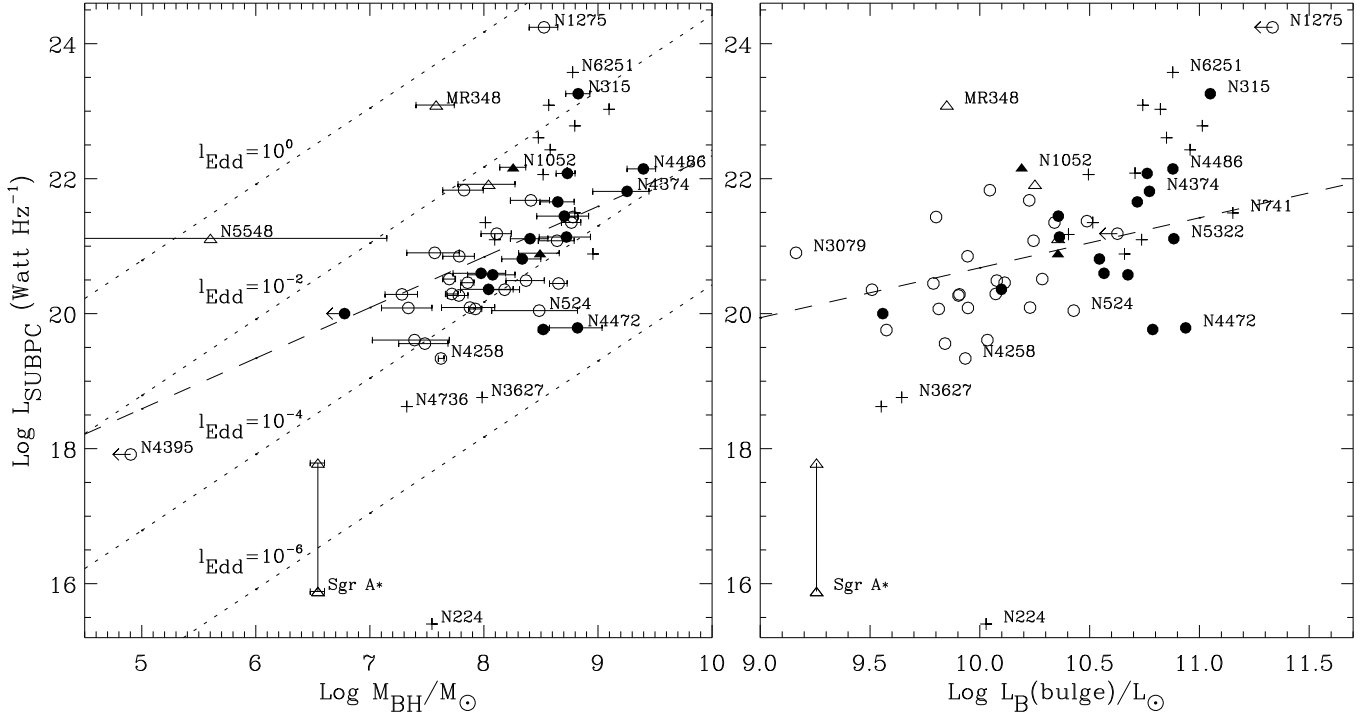


Fig. 4. A plot of sub-parsec radio luminosity versus (left) black hole mass and (right) bulge luminosity of the host galaxy in the B-band. Only radio-detected sources relatively unambiguously identified with the central engine of the AGN (see text) and with radio fluxes measured at resolution better than 1 pc are plotted as circles (Palomar LLAGNs and AGNs) and triangles (other LLAGNs and AGNs). For these, filled symbols are used for elliptical galaxies, and errors in black hole mass are shown (see text). LLAGNs and AGNs (some of which are in the Palomar sample) with radio luminosities measured at resolution between 1 pc and 5 pc are shown as crosses. Two measurements (at different resolutions; Nagar et al., 2002a) are plotted for the Galaxy. The four dotted lines in the left panel represent Eddington ratios (from 10^{-6} to 1) calculated assuming that jet kinetic power dominates the accretion energy output (see Sect. 5.5). The dashed line in the left panel shows a linear fit to the circles and triangles with $\log M_{\text{BH}} > 10^7 M_{\odot}$; the dashed line in right panel shows a linear fit to the circles and triangles except the Galaxy (see text).

1 pc, and available black hole mass measurements or estimates from σ_c . These 6 galaxies are: the Galaxy (Krichbaum et al., 1998), for which as in Nagar et al. (2002a) we plot two radio luminosities: that of only Sgr A* (10 mas or 4×10^{-4} pc resolution) and that for the full Sgr complex; and Seyferts observed with the VLBA/I (from the list compiled in Middelberg et al., 2004): Mrk 348 (Ulvestad et al., 1999), NGC 1052 (Kellermann et al., 1998), NGC 2110, NGC 5252 (Mundell et al., 2000), and NGC 5548 (Wrobel, 2000).

Xu et al. (2000) observed additional (i.e. not in the Palomar Sample) FR Is with the VLBA, but their resolution of ~ 7 mas translates to > 1 pc and only some of these FR Is could be included in the figure as crosses. We do not consider other more powerful radio sources (e.g. blazars) to minimize confusion due to relativistic beaming.

A visual inspection of Fig. 4 shows a rough overall correlation between radio luminosity and both black hole mass and galaxy bulge luminosity. The large scatter in both relationships is possibly due to a large range of accretion rates at any given black hole mass (dotted lines in

Fig. 4 left), which results in widely different output radio luminosities. Statistical tests³ from the ASURV package (Lavalley et al., 1992), suggest that both correlations are statistically significant even when the Galaxy and other nuclei with low black hole mass are removed, as detailed below. The radio luminosity and black hole mass correlation has significance 99.95-99.98% when all circles and triangles in Fig. 4 (left panel) are considered. This significance drops only slightly (98.9-99.8%) when the Galaxy and NGC 4395 are not considered, and is still 98.9-99.8% when only nuclei with $\log M_{\text{BH}} > 10^7 M_{\odot}$ are considered. The correlation between radio luminosity and bulge luminosity has significance 99.3-99.7% when all circles and triangles in Fig. 4 (right panel) are considered. This correlation is still significant (95.6-99.2%) when the Galaxy is not considered. Linear regression analysis by the Buckley James method in ASURV on the circles and triangles in Fig. 4 (not considering the Galaxy in both cases, and using only nuclei with $\log M_{\text{BH}} > 10^7 M_{\odot}$ in the case of the

³ Measurement errors were not considered when running the statistical tests.

relation between radio luminosity and M_{BH} yields:

$$\begin{aligned} \log(L_{\text{Sub-pc}} [\text{W/Hz}]) \\ = 0.74 (\pm 0.31) \log(L_{\text{B(bulge)}}/L_{\odot}) + 13.28 \quad (1) \\ = 0.75 (\pm 0.26) \log(M_{\text{BH}}/M_{\odot}) + 14.84 \end{aligned}$$

These two relations are plotted with dashed lines in Fig. 4.

The relation between radio luminosity and black hole mass has been discussed by several authors, with conflicting results. For example, Franceschini et al. (1998) claimed a correlation with a much steeper slope based on a small number of objects, while Ho (2002) and Woo & Urry (2002) found no correlation for larger samples of AGNs and LLAGNs. We emphasize that our results and those of Ho (2002) and Woo & Urry (2002) are not contradictory given the samples and physical scales of the radio emission. Here, in Fig. 4, we specifically address the correlation between radio emission from the base of the jet or from the innermost accretion inflow (measured here by the sub-parsec radio emission in nuclei for which this radio emission is relatively unambiguously associated with the true ‘core’ rather than with larger scale ‘jets’) and black hole mass or bulge luminosity for a sample dominated by nearby LLAGNs. It is possible that the range of actual Eddington ratios l_{Edd} (which could be responsible for the scatter in radio luminosities at any given black hole mass) is small enough among LLAGNs in our sample to not destroy the correlation between sub-parsec radio luminosity and black hole mass or bulge luminosity. Indeed, the estimated l_{Edd} for the nuclei in Fig. 4 (calculated assuming the jet power, Q_{jet} , dominates the accretion energy output; see Sect. 5.5) spans a relatively narrow range (see points and dashed lines in the left panel of Fig. 4). Ho (2002), on the other hand, used a sample with a larger range of l_{Edd} and measured nuclear radio luminosities at lower resolution ($5''$; or several hundreds of parsecs). Both factors (‘classical’ Seyferts are apparently more likely to produce radio emission on 100-pc scales than LLAGNs; see Sect. 5.4) could have lead to the absence of a correlation between radio luminosity and black hole mass in his sample. Similar factors would also apply to the results of Woo & Urry (2002), who used a sample which covered a larger range of l_{Edd} and which included many powerful (and presumably relativistically beamed) radio sources.

5.3. Radio Luminosity Function

The nuclear (150 mas-scale) 15 GHz RLF for all 68 radio-detected Palomar sample LLAGNs and AGNs (Table 1) is plotted in Fig. 5a as open circles. LLAGNs not detected in the radio have been excluded from the RLF calculation. Only 2 of the radio detections in the Palomar sample (NGC 1275 and NGC 4151) are true AGNs as defined by their emission-line properties i.e. they have $L_{\text{H}\alpha} \gg 10^{40} \text{ erg s}^{-1}$. The HII-region nuclei and absorption-line nuclei, which are excluded from this RLF calculation, have much lower radio luminosities than the LLAGNs and AGNs in the sample. The RLF has been computed via

the bivariate optical-radio luminosity function (following the method of Meurs & Wilson, 1984), after correcting for the incompleteness (Sandage, Tammann, & Yahil, 1979) of the RSA catalog (from which the Palomar sample was drawn). Errors were computed following the method of Condon (1989). We emphasize that the nuclear 15 GHz RLF presented here traces only the inner AGN jet or accretion inflow, and does not include the contribution from >150 mas-scale radio jets.

RLFs at 1.4 GHz and 5 GHz for Palomar Seyferts have been presented in Ulvestad & Ho (2001a), and a RLF (using observations at several frequencies and resolutions) for the complete Palomar sample has also been discussed in Filho (2003, *PhD* thesis). The RLF we present here (first presented in Nagar, 2003) is in rough agreement with the above RLFs given the errors. The advantages of the RLF presented here are threefold. First, it is based on a larger number (68) of radio detections. Second, it is derived from uniform radio data: all except 13 radio detections and 21 radio non-detections have their fluxes or upper limits derived from our 15 GHz (2 cm) VLA A-configuration observations reduced in a uniform way; these 34 exceptions have fluxes or upper limits derived from data of similar resolution and frequency. Third, the radio data were obtained at high resolution and high frequency: both these factors reduce the contamination of star-formation-related emission to the true AGN radio emission, which is especially important at these low AGN luminosities.

At the highest luminosities the Palomar RLF is in good agreement with that of ‘classical’ Seyferts (Fig. 5a), as previously noted by Ulvestad & Ho (2001a). We have plotted the RLFs of Markarian Seyferts (1.4 GHz RLF from Meurs & Wilson, 1984) and of CfA Seyferts (1.4 GHz RLF calculated by Ulvestad & Ho (2001a) using 8 GHz data from Kukula et al. (1995)), after conversion to our values of H_0 and frequency (assuming that the 1.4 GHz emission is optically-thin with spectral index -0.75). Of course, the ‘classical’ Seyfert RLFs are not strictly comparable to ours since our 15 GHz survey detected flat-spectrum emission (Nagar et al., 2001, 2002b) which may have been invisible to the 1.4 GHz observations, and conversely, the 15 GHz observations may not have detected the steep spectrum emission which dominated the 1.4 GHz observations. Furthermore, the AGN-related radio structures in the Palomar LLAGNs are either sub-arcsec (i.e. the nuclear radio emission is the total AGN-related radio emission) or, in a few cases, FR I-like. Neither of these can be easily compared or corrected to the radio structures seen in most Markarian or CfA Seyferts at lower radio frequencies.

At lower luminosities, the sample extends the RLF of powerful AGNs by more than three orders of magnitude. A linear (in log-log space) fit to the Palomar nuclear RLF above $10^{19} \text{ Watt Hz}^{-1}$ (i.e. excluding the two lowest luminosity bins; see below) yields:

$$\log \rho = (12.5 - 0.78 \times \log(L_{15 \text{ GHz}} [\text{W Hz}^{-1}])) \\ [\text{Mpc}^{-3} \text{ mag}^{-1}] \quad (2)$$

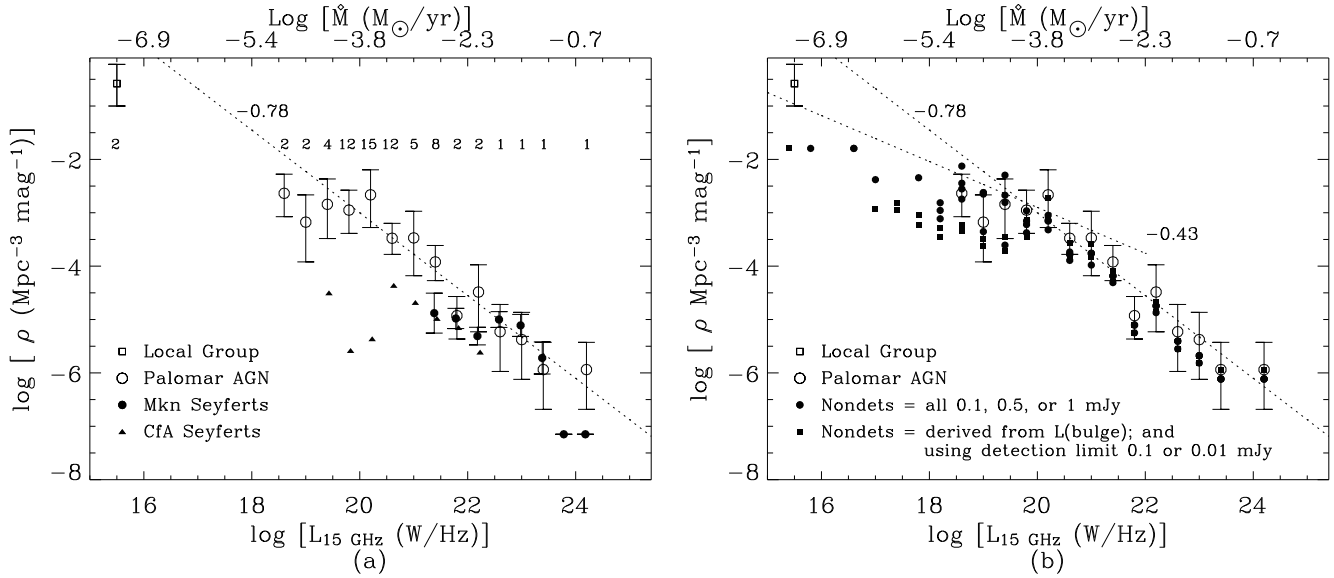


Fig. 5. (a) The 15 GHz radio luminosity function (RLF) of the 150 mas-scale radio nuclei in the LLAGNs and AGNs of the Palomar sample (open circles, with the number of galaxies in each bin listed above the symbol). For a rough comparison (see text) we also plot the 15 GHz RLFs (after converting to our value of H_0 and frequency; see text) of Markarian Seyferts and CfA Seyferts. The dotted line is a power-law (-0.78) fit to the Palomar nuclear RLF (excluding the two lowest radio luminosity points). Also shown is the estimated 15 GHz nuclear RLF of galaxies in the local group (open square, with 2 galaxies; see text). The upper x axes of both panels show the implied logarithm of the mass accretion rate (in $M_\odot \text{ yr}^{-1}$) within the context of a jet model (Falcke & Biermann, 1999), assuming both a 10% energy conversion efficiency, and that the jet kinetic power dominates the accretion energy output (see Sect. 5.5); (b) the axes and open symbols are the same as in (a). The filled symbols show several simulated nuclear RLFs for the Palomar sample which include nuclei not detected in our 15 GHz survey in the RLF calculation (see text for details). The dotted line with slope -0.43 shows a possible fit (made by eye) to the RLF at the lowest luminosities; the other dotted line is the same as in the left panel.

As we discuss below, a potential fit to the RLF below $10^{19} \text{ Watt Hz}^{-1}$ is (with units as in eqn. 2):

$$\log \rho = 5.7 - 0.43 \times \log L_{15 \text{ GHz}} \quad (3)$$

There is some indication of a low luminosity turnover in the Palomar RLF (Fig. 5a). Admittedly, this apparent turnover is partly due to the incompleteness of the radio survey, i.e. biased by the sub-milli-Jansky population which remains undetected. Nevertheless there are several reasons to believe the presence of such a turnover, as detailed below and in Fig. 5b. First, and most convincingly, one runs out of bright galaxies: an extension of the -0.78 power law fit to lower luminosities would require e.g. an LLAGN like Sgr A* or M 31* to be present in every Mpc^{-3} . However, there are only about 318 known non-irregular galaxies at $D < 10 \text{ Mpc}$ of which only 70 have $\log (L/L_\odot) > 9$ and only 22 have $\log (L/L_\odot) > 10$ (Karachentsev, Makarov, & Huchtmeier, 1999). To better determine the RLF shape at lower luminosities, we have calculated an approximate RLF⁴ for the nuclei of the local group of galaxies. The local group has 13 galaxies with

⁴ Here we use the highest resolution radio flux, instead of a ‘matched’ linear-resolution flux. The latter flux is dominated by extra-nuclear (non-AGN related) emission for these lowest luminosity AGNs and is thus not directly comparable to the

$M_v < -14.8$, of which 6 are classified as Irregular. The remaining 7 have been surveyed at high resolution with the VLA to detection limits between $30 \mu\text{Jy}$ and 1 mJy . Our Galaxy ($\sim 1 \text{ Jy}$ for Sgr A*; Krichbaum et al., 1998) and M 31 (0.033 mJy Crane et al., 1993) have nuclear radio luminosities $\sim 10^{15} \text{ Watt Hz}^{-1}$, and the other five all have upper limits to their nuclear radio flux: M 32 (NGC 221, $< 0.03 \text{ mJy}$; Ho et al., 2003b), NGC 185 ($< 0.12 \text{ mJy}$; Ho & Ulvestad, 2001), NGC 147 and NGC 205 ($< 1 \text{ mJy}$; Heckman, Crane, & Balick, 1980), and NGC 598 ($< 0.03 \text{ mJy}$ from our reduction of 8.4 GHz A-configuration VLA archive data from project AC342). We calculate the local group RLF using a simple V/V_{max} test for the Galaxy and M 31, assuming a detection limit of $30 \mu\text{Jy}$. This local group point, plotted as an open square in Fig. 5a and b, is also consistent with a low-luminosity break in the overall RLF. The error bar on the local group RLF point is from Poisson statistics; the true error, from the generalization of our (a-posteriori) local group properties, is likely to be larger.

As a further test we simulated the shape of the Palomar RLF at low luminosities by converting some or all of the LLAGNs not detected in our 15 GHz survey radio fluxes of the other more luminous radio sources used in the RLF computation.

into radio detections as follows (a total of 6 simulated RLFs; filled symbols in Fig. 5b). We first recomputed the RLF assuming that all 125 radio non-detected LLAGNs had radio nuclei with flux 0.5 mJy and using this value as the assumed detection limit of the survey. We then recomputed the RLF for the three cases that the non-detected Seyferts and LINERs (71 nuclei) all had radio nuclei with flux 1 mJy, 0.5 mJy, or 0.1 mJy (and using the corresponding flux as the assumed detection limit of the survey). The above four simulated RLFs are plotted with filled circles in Fig. 5b. To explore two more possibilities, we set the radio flux of individual non-detected LLAGNs to the values expected from the rough proportionality between bulge luminosity and 150 mas-scale radio luminosity for nearby galaxies (dashed line in Fig. 18, lower panel, of Nagar et al., 2002a). We then recomputed the RLF for two assumed detection limits (0.1 mJy and 0.01 mJy) and ensured that the estimated fluxes fell in the range between 1 mJy (our survey’s actual detection limit) and the assumed detection limit (if the estimated flux was lower than the assumed detection limit then the nucleus continued to be treated as a non-detection). The resulting two simulated RLFs, calculated from a total of 98 and 170 radio detections, respectively, are plotted with filled squares in Fig. 5b. All the simulated RLFs support a low luminosity break in the Palomar RLF. The actual shape of the low end of the RLF is uncertain and in Fig. 5b and Eqn. 3 we show a potential power law fit which satisfies the current data and extrapolations.

5.4. Sub-parsec Jets

About 20 of the 44 sources in Table 2 have detected sub-parsec scale (and/or sometimes larger scale) ‘jets’. These include NGC 315 (Cotton et al., 1999b; Fomalont et al., 2000; Giovannini et al., 2001), NGC 1167 (Giovannini et al., 2001, this work), NGC 1275 (Dhawan, Kellerman, & Romney, 1998; Walker et al., 2000), NGC 2273 (this work), NGC 3031 (M 81; Bietenholz et al., 2000), NGC 3079 (Trotter et al., 1998), NGC 4151 (Mundell et al., 2003; Ulvestad et al., 1998), NGC 4258 (Herrnstein et al., 1997), NGC 4261 (e.g. Jones et al., 2001), NGC 4278 (Jones et al., 1984; Falcke et al., 2000), NGC 4374 (M 84; Wrobel et al., 1996, this work), NGC 4486 (M 87; Junor & Biretta, 1995), NGC 4552 (M 89; Nagar et al., 2002a), NGC 4589 and NGC 5353 (this work), NGC 5354 (Filho et al., 2004), NGC 5363 (this work), NGC 5846 (Filho et al., 2004), NGC 6500 (Falcke et al., 2000), and NGC 7626 (this work, also tentatively detected by Xu et al., 2000).

The mas-detected radio nuclei fit into four categories, with Seyferts and LINERs preferentially belonging to one or the other category: (a) powerful radio galaxies or low power radio galaxies – NGC 315, NGC 1275, NGC 4261, NGC 4374, NGC 4486 and NGC 7626 – which have an elliptical host, a LINER nuclear spectrum, and collimated sub-parsec to kpc jets; (b) nuclei which do not have de-

tected parsec-scale jets, but have larger (100 pc- or kpc-scale) jets. These are preferentially Seyfert-like nuclei (6 nuclei) though NGC 5363 (LINER) and NGC 5846 (transition nucleus) fall in this class; (c) nuclei with detected sub-parsec jets but weak or no known larger scale jets – preferentially in LINERs or transition nuclei. These nuclei – NGC 4278, NGC 4552, NGC 4589, NGC 5353, NGC 5354, and NGC 6500 – typically show curved or highly bent jets (Nagar et al., 2002a; Filho et al., 2004, this work) and proper motion studies (Nagar et al., in prep) suggest that these jets are frustrated in the inner few parsecs; (d) the remaining ~ 23 nuclei in Table 2 do not show extended mas-scale emission but require more detailed study of their 100 pc to kpc scale radio emission. The disappearance of the larger-scale jet in category (c) above, and the morphology of their parsec-scale jets (highly curved or bent) suggests that the jet does not propagate beyond the inner few parsecs, either due to being uncollimated, or because of interaction with the ambient medium. If this is the case, the energy deposited into the inner few parsecs by the jet (next section) is significant, and could potentially be responsible for lowering the larger scale (i.e. outside the accretion disk) gas inflow and thus ultimately the accretion rate.

5.5. Jet Power versus Radiated Luminosity

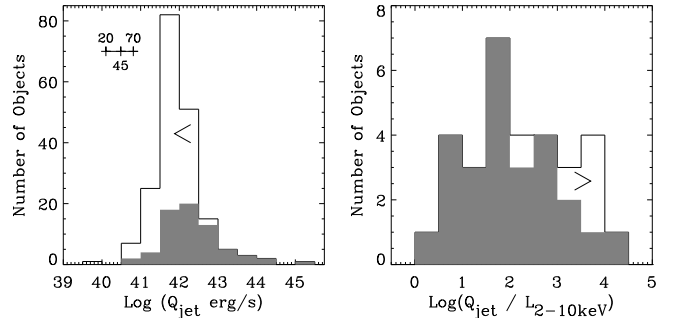


Fig. 6. Left: the implied ‘minimum jet power’, (Q_{jet}) of the radio-detected (grey shaded area) and radio non-detected (white area) LLAGNs and AGNs, calculated from the peak VLA 15 GHz flux using Eqn. 20 of Falcke & Biermann (1999) and assuming a jet inclination of 45° to the line of sight. The inset illustrates the range of calculated minimum jet kinetic powers for three assumed inclinations: 20° , 45° , and 70° . **Right:** log of the ratio of minimum jet power (assuming 45° jet inclination) to X-ray luminosity (in the 2–10 keV band) for radio detected LLAGNs and AGNs. The grey and white histograms represent LLAGNs/AGNs with detected, and upper limits to, the hard X-ray emission, respectively.

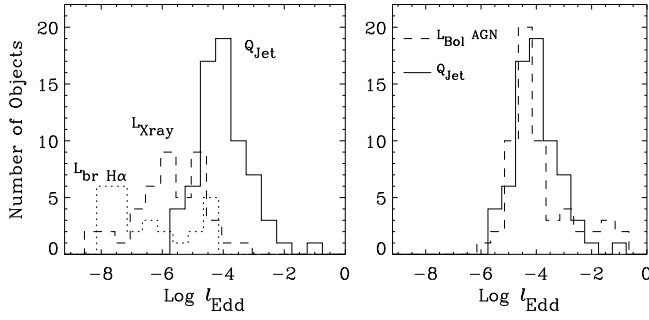


Fig. 7. A comparison of the kinetic and radiated accretion power outputs as a fraction of $L_{\text{Eddington}}$ in four energetically important wavebands. In both panels the histograms are offset by 0.1 in x for clarity. **Left:** histograms of the broad $H\alpha$ luminosity (dotted line), hard X-ray luminosity (2–10 keV; dashed line), and minimum jet power (Q_{jet} ; solid line) for all broad line nuclei, all hard X-ray detected nuclei, and all radio detected nuclei, among the LLAGNs and AGNs of the Palomar Sample, respectively. **Right:** histograms of the minimum jet power (Q_{jet} ; solid line) and radiated bolometric luminosity (derived from the [O III] luminosity, see text; dashed line) for the radio detected nuclei in the LLAGNs and AGNs of the Palomar Sample.

5.5.1. Jet Power Domination in Palomar LLAGNs

With an estimated black hole mass and an emitted luminosity, one can estimate the Eddington ratio, i.e. $l_{\text{Edd}} = L_{\text{Emitted}}/L_{\text{Eddington}}$. Previous calculations of l_{Edd} for LLAGNs have considered only the radiated component of L_{Emitted} . Since LLAGNs lack a ‘big blue bump’, the X-ray emission has been thought to dominate the bolometric luminosity (Ho, 1999). With most LLAGNs having hard X-ray luminosities of only $\sim 10^{40}$ erg s $^{-1}$ or lower, the accretion is inferred to be highly sub-Eddington (Ho et al., 2001; Terashima & Wilson, 2003; Filho et al., 2004).

If, as justified above, the compact radio nuclei and sub-parsec jets represent emission from the base of a relativistic jet launched close to the black hole, then the kinetic energy in the jet can be quite high. Equation 20 of Falcke & Biermann (1999) - assuming an average inclination of 45° - can be used to obtain ‘minimum jet powers’ (Q_{jet}) of $10^{40} - 10^{45}$ erg s $^{-1}$ (Fig. 6, left panel) from the 15 GHz peak VLA flux of radio detected LLAGNs. For LLAGNs with both hard X-ray and radio luminosity available, this jet power greatly exceeds the radiated X-ray luminosity (Fig. 6, right panel). Since the bolometric luminosity (L_{Bol}) in electromagnetic radiation is estimated to be only $\sim 3 - 15 \times L_{0.5-10 \text{ keV}}$ for LLAGNs (Ho, 1999), this suggests that the accretion power output is dominated by the jet power. This domination of jet power over X-ray emission is analogous to the situations for $\sim 10\text{--}15 M_\odot$ black holes in Galactic X-ray binary systems (Fender, Gallo, & Jonker, 2003) and for powerful radio galaxies (e.g. Celotti & Fabian, 1993; Owen, Eilek, & Kassim, 2000).

To expand on this issue, we compare the estimated minimum jet power to the observed hard X-ray luminosity and emission-line luminosities for the Palomar sample LLAGNs. Clearly (Fig. 7, left) the minimum jet power is significantly larger than the measured hard X-ray luminosity (as noted above) and the luminosity in broad $H\alpha$. On the other hand, if the radiated bolometric luminosity is estimated from the [O III] luminosity - from the empirical result that the spectral energy density of type 1 AGNs typically shows $L_{\text{Bol}} = 3500 \times L_{[\text{O III}]}$ (Heckman et al., 2004, see also next Sect.) - then LLAGNs show similar distributions of minimum jet power and radiated bolometric luminosity (Fig. 7, right).

5.5.2. A Common Jet-Power Scaling for LLAGNs and Powerful AGNs

The radio detected LLAGNs in the Palomar sample (circles; Fig. 8) fall nicely at the low luminosity end of the correlation between jet kinetic power and total emission line luminosity from the narrow line region (NLR) for more powerful FR I and FR II galaxies. This figure includes FR I and FR II radio galaxies (slanted crosses; in these the jet kinetic power is estimated from lobe-feeding energy arguments; Rawlings & Saunders, 1991) and other powerful radio sources (including BL Lacs, quasars, and radio galaxies) with parsec-scale jets (crosses; in these the bulk kinetic energy in the jet was estimated using a self-Compton synchrotron model applied to the parsec-scale jet; Celotti & Fabian, 1993). We estimated the NLR luminosity for the Palomar LLAGNs and AGNs following Celotti & Fabian (1993):

$$L_{\text{NLR}} = 3 \times (3 L_{[\text{O II}]\lambda 3727} + 1.5 L_{[\text{O III}]\lambda 5007})$$

with $L_{[\text{O II}]\lambda 3727}$ estimated as $0.25 \times L_{[\text{O III}]\lambda 5007}$ for Seyferts and $3 \times L_{[\text{O III}]\lambda 5007}$ for LINERs and transition nuclei. The Palomar [O III] luminosities were measured in a $2'' \times 4''$ nuclear aperture (Ho et al., 1997a); these values closely approximate the total NLR luminosity in most nuclei except a handful, e.g. NGC 4151, which have more extended NLRs.

5.5.3. LLAGN Jet-Power and Global Energetics

The energetics of the jet are also important in the context of so called cooling flows and in regulating the feedback between galaxy growth and black hole growth. For example, in many clusters the central cD galaxy has an FR I radio morphology, with the radio jet playing an important role in the above issues and in the global energetics of the cluster gas (Owen, Eilek, & Kassim, 2000; Binney, 2004b; Ostriker & Ciotti, 2004). A comparison of the jet kinetic power with the power injected into the ISM by supernovae types I and II in the host galaxies is shown in Fig. 9 for the radio detected Palomar LLAGNs/AGNs. The supernova rates (as a function of galaxy morphological type) are taken from the ‘Case B’ values in Table 6 of van den Bergh & McClure (1994), e.g. 0.25 SNU for E and

S0 galaxies (all from SN type Ia), where 1 SNU = 1 SN per century per $10^{10}(L_B/L_\odot)$. The total SN rate is slightly higher in later type galaxies due to the contribution of SN type II. Values of L_B/L_\odot were taken from Ho et al. (1997a) and each supernova is assumed to inject 10^{51} erg of kinetic energy into the ISM (e.g. Binney & Tremaine, 1987; Pellegrini & Ciotti, 1998). The jet power is clearly the major player in the nuclear energetics not only because it exceeds the total SN kinetic power in almost all cases, but also because its nuclear origin allows a closer ‘feedback’ to the accretion inflow. A significant fraction of the jet energy is potentially deposited in the central parsecs, especially in LLAGNs which show pc-scale (usually bent) jets but no larger scale jets (Sect. 5.4); such deposition of jet power can considerably slow down or balance any cooling flow or other inflow in the inner parsecs and thus ultimately help ‘starve’ the accretion disk (e.g. Di Matteo et al., 2001). Additionally, LLAGNs with kpc-scale jets inject significant energy into the inter-galactic medium (IGM), and work against any cooling flow (see e.g. Pellegrini & Ciotti, 1998). The most recent of such ‘feedback’ analyses (Binney, 2004b) does take into account the jet power, though for the more powerful FR I type jets in cD galaxies. Our results show that their models can be applied, at least qualitatively, to LLAGNs.

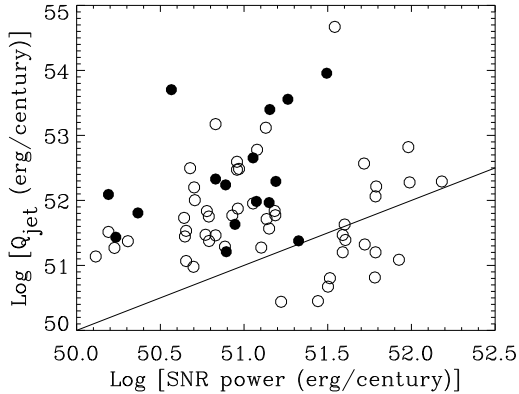


Fig. 9. A comparison of the ‘minimum jet power’ (Q_{jet}) and the kinetic energy injected into the ISM by supernovae type I and II for the radio detected Palomar LLAGNs and AGNs. Filled circles are used for elliptical galaxies. The solid line shows the line of equality.

In summary, Eddington ratios, l_{Edd} , calculated from hard X-ray luminosities heavily underestimate the true accretion power output in LLAGNs. This finding is in line with that for more powerful radio galaxies, where the jet kinetic power is two to five orders of magnitude larger than the radiated radio luminosity, and often significantly larger than the total radiated bolometric luminosity (Celotti & Fabian, 1993; Owen, Eilek, & Kassim, 2000). Using $L_{\text{Bol}} = 3500 L_{[\text{OIII}]}$ or $L_{\text{Bol}} = Q_{\text{jet}}$ yields similar distributions of L_{Bol} . This, and the scaling between L_{NLR}

and Q_{jet} , argues for a common central engine in all AGNs from LLAGNs to powerful FR IIs, but with the caveat that the $[\text{OIII}]$ luminosity in LLAGNs is potentially contaminated by non accretion related processes. Finally, the jet is potentially a significant (maybe even dominant) source of heating in the galaxy. If the jet is disrupted in the inner parsecs, then the jet power could play a role in slowing any cooling flow or other accretion inflow on parsec-scales, thus starving the accretion disk.

5.6. The Eddington Ratio

In the previous section we showed that the accretion energy output in LLAGNs with radio nuclei is dominated by the jet power, and is of the order of $l_{\text{Edd}} = 10^{-6}$ to 10^{-2} . Here we look at the dependence of this jet-power-derived l_{Edd} on other quantities.

Heckman et al. (2004) have investigated black hole and galaxy growth using 23,000 type 2 AGNs from the Sloan Digital Sky Survey (SDSS). They use σ_c to estimate black hole mass, and $L_{\text{Bol}} = 3500 L_{[\text{OIII}]}$. They find that most present-day accretion occurs onto black holes with masses $< 3 \times 10^7 M_\odot$, and that most black hole growth takes place in systems with accretion rate less than one fifth of the Eddington rate. It is interesting to apply their analysis to the Palomar LLAGNs since these objects have emission-line luminosities typically ten to a hundred times fainter than the SDSS AGNs. The Palomar LLAGNs show a different behavior to the SDSS AGNs: the numerous Palomar LLAGNs with low black hole masses are accreting a similar mass per year as the fewer Palomar LLAGNs and Palomar AGNs at higher radio luminosity. This is true whether the accretion rate is calculated from the $[\text{OIII}]$ luminosity, as in Heckman et al. (2004), or from Q_{jet} (e.g. Fig. 5, upper x -axis).

The Palomar sample ellipticals (filled symbols in Fig. 10) show a strong correlation between Eddington ratio, l_{Edd} (calculated assuming the jet power dominates the accretion energy output) and all of emission-line luminosity, radio luminosity, and the ratio of radio luminosity to emission line luminosity. Among the non-elliptical nuclei (open symbols in Fig. 10), Seyfert nuclei (triangles) display higher Eddington ratios than LINERs (circles), even though the distribution of radio luminosities (from which Q_{jet} is calculated) is similar for the two classes. This is most clearly noticeable in Fig. 10c.

5.7. Discovery of LLAGNs: A Comparison of Radio, Optical, and X-ray Methods

The current study and sample allows a comparison of the relative success of deep optical spectroscopy, high resolution radio imaging, and (to some extent) hard X-ray imaging, in identifying low-luminosity accreting black holes. Such a comparison is specially relevant in view of the several hundred thousand AGNs and LLAGNs being identified by current large surveys out to $z \sim 6$. We consider

three factors here: efficiency, reliability, and completeness. In this subsection, we shall use the term “AGN” to mean “AGN + LLAGN”, namely objects powered by accretion onto a supermassive black hole.

The optical spectroscopy (of ~ 486 nuclei) was obtained at the 5 meter Hale telescope with typical exposures of 30 min to 1 hr per nucleus. Has this optical spectroscopy missed any (radio- or X-ray identified) AGNs in the Palomar sample? The spectroscopic survey found emission-lines in all except 53 nuclei (Ho, Filippenko, & Sargent, 2003a). Of these 53 absorption line nuclei we found only two with radio nuclei which would identify them as definite AGNs, and a further three to five with radio nuclei possibly related to an AGN (see the appendix). We could not find reliable hard X-ray identifications of AGNs, for lack of data, in any of the absorption line nuclei. The H II nuclei in the Palomar sample also show no indication of an AGN in the radio (Ulvestad & Ho, 2001b) or X-ray. Thus, the optical spectroscopic survey has missed only two definite (and perhaps three or five probable) AGNs which would have been picked up by a radio survey with detection limit ~ 1 mJy. The reliability of AGN identification from optical spectroscopy alone is hard to quantify. At these low luminosities, emission lines could be powered by sources other than an AGN, e.g. a nuclear starburst (Maoz et al., 1998).

The radio imaging (of ~ 200 nuclei) was done with the VLA with typical integration times of 10 to 15 min per nucleus. Follow-up VLBA imaging (1 hr per nucleus) showed that the VLA-only imaging could be used for reliable identification of the radio nuclei as AGN-related (Sect. 4.2). The high brightness temperature radio nuclei and parsec-scale jets, found through VLBA observations, are the most reliable indicators of AGNs in these nuclei as a class. Our radio imaging has identified fewer AGN candidates than the optical spectroscopy, though it is likely that deeper radio imaging will uncover significantly more AGNs (Nagar et al., 2002a). It is difficult to ascertain whether the radio survey has missed any (definite) optically identified AGNs, since the detection of weak emission lines does not guarantee the presence of a low-luminosity accretion-powered nucleus. Ideally, one requires hard X-ray confirmation of the presence of an AGN: this issue will be more fully discussed in Terashima et al., (in prep.). The cumulative number of ‘definite’ AGNs identified by the optical spectroscopic and the radio imaging methods, as a function of the luminosity in the narrow $H\alpha$ line, is shown in Fig.11. Here we use the presence of either a nuclear hard X-ray source (solid lines; Fig. 11) or broad $H\alpha$ emission (dashed lines; Fig. 11) as the signpost of a ‘definite’ AGN - i.e. an object powered by accretion onto a supermassive black hole. Our radio survey has detected 26 of 39 (66%) of the type 1 nuclei in the sample. Of the 14 type 1 nuclei not detected in our radio survey, all 5 Seyferts were found to have radio nuclei in the deeper radio survey of Ho & Ulvestad (2001), while the nature of the others is unknown.

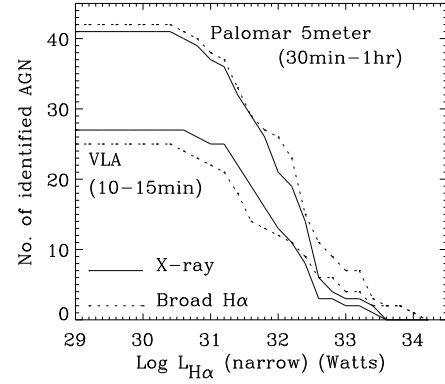


Fig. 11. The cumulative number of ‘definite’ (solid lines for nuclei with a hard X-ray nuclear source and dashed lines for type 1 nuclei, i.e. with broad $H\alpha$ emission) AGNs identified by optical spectroscopy (upper two lines; ~ 30 min to 1 hr on the Palomar 5 meter) and radio imaging (lower two lines; ~ 10 –15 min at the VLA), as a function of the luminosity of the narrow $H\alpha$ line.

In summary, optical spectroscopy of the Palomar sample has found almost all radio or X-ray identified AGNs to have emission-lines: as discussed in the Appendix, very few of the nuclei with only absorption lines have radio emission likely powered by an accreting black hole. A caveat here is that the absorption line nuclei have not been surveyed in precisely the same way as we have surveyed the AGNs and LLAGNs. The optical spectroscopic method also finds many nuclei with emission lines powered by hot stars (H II nuclei) and these emission lines can hide weaker emission lines from an AGN. High resolution, high frequency radio imaging (the present survey) has detected a smaller fraction of AGN candidates in the Palomar sample than the optical spectroscopic method, but we have argued that these radio sources are not related to stellar processes. Thus, the presence of a compact flat-spectrum high brightness-temperature radio core is a more reliable indicator of an accreting black hole than the presence of optical emission lines, at least at these low emission line and radio luminosities. A hard X-ray nucleus is also an ideal signpost of an AGN. However, high resolution (i.e. *Chandra*) is required to minimize confusion with X-ray binaries or Ultraluminous X-ray sources (ULXs), which have similar luminosities to the AGN in LLAGNs. Further, a large X-ray survey is very expensive in terms of telescope time. Instead, scientific results can be efficiently attained by hard X-ray observations of subsamples selected to have a compact radio core (Terashima & Wilson, 2003, Terashima et al., in prep.).

6. Discussion

The VLBI results (Sect. 4.2 and Table 2) confirm that almost all (38 of 39, or 97%) LLAGNs and AGNs in the Palomar sample with $S_{15\text{GHz}}^{\text{VLA}} > 2.7$ mJy have

detected mas-scale or sub mas-scale radio nuclei with brightness-temperature $\gtrsim 10^7$ K. The only exception is NGC 2655: this nucleus has a steep spectrum at arc-sec resolution (Nagar et al., 2000) and was not detected by us with the VLBA. Deeper VLBA/I maps show mas-scale radio nuclei in five Palomar LLAGNs with $S_{15\text{ GHz}}^{\text{VLA}} \leq 2.7$ mJy (Table 2). It is notable that the LLAGNs and AGNs with known ultracompact radio nuclei are divided between Seyferts and LINERs in proportion to their relative numbers in the Palomar sample (14 and 23, respectively; see Table 2). Thus the probability of detecting ultracompact radio nuclei in LLAGNs with Seyfert and LINER spectra is similar. Nuclear starbursts have a maximum brightness-temperature of $\sim 10^{4-5}$ K (Condon et al., 1991) while the most luminous known radio supernova remnants (e.g. Colina et al., 2001) would have brightness temperatures $\leq 10^7$ K even if they were ≤ 1 pc in extent. As argued in Falcke et al. (2000), if the nuclear radio emission is attributed to thermal processes, the predicted soft X-ray luminosities of LLAGNs would be at least two orders of magnitude higher than observed by *ASCA* (Terashima, Ho, & Ptak, 2000) and *Chandra* (Ho et al., 2001; Terashima & Wilson, 2003; Filho et al., 2004). Also, as pointed out by Ulvestad & Ho (2001a), single SNRs (Colina et al., 2001) or a collection of SNRs (Neff & Ulvestad, 2000) would have radio spectral indices (defined by $S \propto \nu^\alpha$) $\alpha \sim -0.7$ to -0.4 rather than the values $\alpha \sim -0.2$ to 0.2 seen in the VLBA-detected LLAGNs (Nagar et al., 2001, 2002b; Anderson, Ulvestad, & Ho, 2004; Nagar et al., in prep). Furthermore, significant flux variability is observed (Nagar et al., 2002a). Thus, the only currently accepted paradigm which may account for the sub-parsec radio nuclei is accretion onto a supermassive black hole. In this case, the mas-scale radio emission is likely to be either emission from the accretion inflow (Narayan et al., 2000) or synchrotron emission from the base of the radio jet launched by the accreting supermassive black hole (Falcke & Biermann, 1999; Zensus, 1997). The latter model is supported by the presence of sub-parsec size jets in many of the nuclei, and the radio spectral shape (Nagar et al., 2001, 2002a,b; Anderson, Ulvestad, & Ho, 2004).

The radio results imply that a large fraction (perhaps all) of LLAGNs have accreting massive black holes. If we consider only the detections of mas-scale radio sources, then at least $25\% \pm 5\%$ of LINERs and low-luminosity Seyferts have accreting black holes. VLA-detected compact radio nuclei with flux < 2.7 mJy were not investigated with the VLBA; in other respects these nuclei are similar to those with detected mas scale structure. Thus it is likely that *all* LLAGNs with VLA-detected compact radio nuclei ($42\% \pm 7\%$ of LINERs and low-luminosity Seyferts) have accreting black holes. The scalings between radio luminosity, emission-line luminosity, and galaxy luminosity (Ulvestad & Ho, 2001a; Nagar et al., 2002a; Filho et al., 2004) provide evidence that the radio non-detections are simply lower luminosity versions of the radio detections.

In fact we find no reason to disbelieve that *all* LLAGNs have an accreting black hole.

Interestingly, ultracompact radio nuclei (Table 2) are found almost exclusively in massive ($M_{\text{B}}(\text{total}) \leq -20$) ellipticals and in type 1 LLAGNs, or both. For massive ellipticals, the high bulge luminosity and black hole mass appear to be key factors related to the production of a radio nucleus, in light of the scalings seen between radio luminosity and these parameters (see Fig. 4 of present paper and Nagar et al. 2002a). Among non-ellipticals, the preferential detection of type 1 LLAGNs may result from the limited sensitivity of optical and radio observations, which detect broad $\text{H}\alpha$ and radio nuclei in only the more luminous LLAGNs. For example, it may be that type 1 LLAGNs are in an outburst phase during which they temporarily host both broad $\text{H}\alpha$ emission and a compact radio nucleus. Type 2 LLAGNs, on the other hand, may harbor quiescent AGNs which do not generate sufficient ionizing photons to power the optical emission lines (e.g. Terashima, Ho, & Ptak, 2000; Filho et al., 2004). Instead, their emission lines could be powered by star formation related processes (Maoz et al., 1998). As another alternative, one can invoke the unified scheme (Antonucci, 1993) and posit that all LLAGNs have accreting black holes and either (a) the radio emission in type 1 LLAGNs is beamed (weakly relativistic jets [$\gamma \sim 2$] can give boost factors of up to ~ 5) and/or (b) the 15 GHz radio emission in type 2 LLAGNs is free-free absorbed by a ‘torus’-like structure i.e. $\tau_{15\text{ GHz}} \geq 1$.

The radio and emission line properties of LLAGNs in elliptical galaxies are consistent with them being scaled-down FR Is (Sect. 5.1 and Sect. 5.5), confirming earlier such suggestions with smaller samples (Nagar et al., 2002a; Verdoes Kleijn et al., 2002; Chiaberge et al., in prep.). Additionally, in the context of jet models, the same scaling relationship between jet kinetic power and radiated NLR luminosity is followed by parsec-scale jets in LLAGNs as kpc-scale jets in powerful FR I and FR II radio galaxies (Fig. 8 and Sect. 5.5).

The nuclear environments of low-luminosity Palomar Seyferts are richer in gas than those of Palomar LINERs (Ho, Filippenko, & Sargent, 2003a), as inferred from higher electron densities (n_e) and higher internal extinction in the former class. We have found that among non-elliptical hosts, LINER nuclei have lower Eddington ratios than Seyfert nuclei (Fig. 10 and Sect. 5.6). Also, we find evidence for a higher incidence of parsec-scale radio jets in LINERs than Seyferts (Sect. 5.4); at least some low luminosity Seyferts do show larger (100 pc scale) jets. It is tempting to speculate, in analogy to Galactic black hole candidates (Fender & Belloni, 2004), that LINERs with radio nuclei are in a ‘low/hard’ state (low Eddington ratio, lack of inner accretion disk, more efficient at launching collimated jets) while low-luminosity Seyferts are in a ‘high’ state (higher Eddington ratios, less efficient at launching collimated jets).

Luminous Seyferts, the Palomar sample, and the local group of galaxies together allow an estimate of the nuclear

radio luminosity function over the radio luminosity range $10^{15} - 10^{24}$ Watt Hz $^{-1}$, more than five orders of magnitude larger than previous AGN samples. At the lowest luminosities there is tentative evidence for a turnover in the RLF. One must therefore reach as far down as the LLAGN regime (but not necessarily lower) to completely study the demographics of nuclear accretion. This point is especially important since larger surveys, e.g. SDSS, probe accretion in AGNs with l_{Edd} one or two orders of magnitude larger than that in the Palomar sample LLAGNs.

When only the radiated luminosity is considered, LLAGNs have very low inferred Eddington ratios. This requires either a very low mass accretion rate or a radiatively inefficient accretion mechanism or both, and was among the original motivations for invoking RIAFs in LLAGNs (but see Binney, 2004a, for an argument against the existence of RIAFs). Including the jet power (Sect. 5.5) in the accretion output weakens the motivation for a RIAF. First, including the jet kinetic power significantly increases the total (radiated plus kinetic) L_{Emitted} and thus the Eddington ratio. Second, the energy deposited by the jet into the nuclear regions can potentially heat the gas in the inner parsecs and thus decrease gas supply to the accretion disk (Sect. 5.5.3). Together these two factors weaken the previous preference for RIAFs over a matter-starved accretion disk plus jet system. The absence in LLAGNs of the ‘big blue bump’ and Fe K α lines are thus the main remaining motivations for preferring an optically-thin, geometrically thick and advection dominated inner accretion structure over the standard optically-thick, geometrically thin accretion disk.

Jet models indicate that the dominant form of power output in LLAGNs is the kinetic power of the jet (Sect. 5.5). The Eddington ratios found are $l_{\text{Edd}} \sim 10^{-2}$ to 10^{-6} (Figs. 4, 7, 10). In terms of a mass accretion rate (assuming a 10% conversion efficiency) this translates to $\dot{M} = 10^{-1}$ to 10^{-5} M_{\odot} yr $^{-1}$ (upper x -axis of Fig. 5). The summed mass accretion rate for all Palomar LLAGNs and AGNs in Fig. 5 is $0.4 M_{\odot}$ yr $^{-1}$. Now, the idealised jet model of equation (20) of Falcke & Biermann (1999) predicts $\log Q_{\text{jet}} \propto 0.79 \times \log L_{\nu}$ (where L_{ν} is the observed luminosity at radio frequency ν) for a jet inclination of 45° , while the Palomar RLF has the form $\log \rho \propto -0.78 \times \log L_{15\text{GHz}}$. While there are large uncertainties in applying the jet model, it is worth remarking that these scalings imply $Q_{\text{jet}} \propto \rho^{-1}$. This implies (since $Q_{\text{jet}} \propto \dot{M}$ under the assumption that the jet power dominates the accretion power output) that the more numerous nuclei with lower radio luminosity are together accreting the same mass per year as the fewer nuclei at higher radio luminosity, at least down to the probable RLF turnover at $\log L_{15\text{GHz}} \simeq 19$ Watt Hz $^{-1}$. Finally, with individual jet powers of $\sim 10^{40} - 10^{45}$ erg s $^{-1}$, LLAGN jets provide a significant source of energy (Sect. 5.5) into the galactic ISM and also perhaps the IGM. As discussed in Di Matteo et al. (2001) a fraction of this jet power deposited within the central ~ 0.1 kpc would be sufficient to

significantly lower the accretion rate at least in the case of spherical accretion.

7. Conclusions

We have presented the results of our VLA plus VLBA radio survey of 162 LLAGNs and AGNs from the Palomar sample of nearby bright northern galaxies. These data have been supplemented by data and results from two other recent surveys, one by Ho & Ulvestad (2001), Ulvestad & Ho (2001a) and Anderson, Ulvestad, & Ho (2004) and the other by Filho et al. (2000) and Filho et al. (2004). The completion of uniform high resolution radio surveys of the LLAGNs and AGNs in the Palomar sample of nearby bright galaxies has yielded the following main results:

- a) 97% (38 of 39) of the LLAGNs and AGNs (with $S_{\text{VLA}}^{15\text{GHz}} > 2.7$ mJy) investigated at mas resolution with the VLBA have pc-scale nuclei with brightness temperatures $\gtrsim 10^{6.3}$ K. Of these nuclei, the ones with the highest nuclear flux densities typically show pc-scale jets. The luminosity, brightness temperature, spectrum, morphology, and variability of the radio emission all argue against an origin in star-formation related processes or as thermal emission. Thus, the nuclear radio emission probably originates either in an accretion inflow onto a supermassive black hole or from jets launched by this black hole-accretion disk system. The latter explanation is supported by the radio morphologies (e.g. Falcke et al., 2000; Nagar et al., 2002a), radio flux variability (Nagar et al., 2002a), and the radio spectral shapes (Nagar et al., 2001, 2002b);
- b) there is no reason to believe that the remaining LLAGNs with compact radio nuclei (investigated at 150 mas resolution) are different from the LLAGNs investigated at mas resolution. Thus, at least half of all LINERs and low-luminosity Seyferts probably contain accreting black holes. The incidence for transition nuclei is much lower;
- c) compact radio nuclei are preferentially found in massive ellipticals and in type 1 nuclei (i.e. nuclei in which broad H α emission is present). The preferential detection of type 1 nuclei could result: 1) from observational selection effects, in which broad H α and radio nuclei have been found in only the more powerful LLAGNs, 2) if only the type 1 LLAGNs are bona-fide AGNs, or 3) if the unified scheme applies and the radio emission from type 1 nuclei is beamed perpendicular to the plane of obscuring material and/or type 2 nuclei are free-free absorbed by the obscuring disk in the radio;
- d) the radio luminosity of the compact nucleus is correlated with the galaxy luminosity and the luminosity and width of the nuclear emission lines (Nagar et al., 2002a). These trends suggest that we have detected only the brighter LLAGNs, i.e. the true incidence of accreting black holes in LLAGNs is higher than found by our survey;
- e) The nuclear radio and nuclear emission-line properties

of LLAGNs fall close to the low-luminosity extrapolations of more powerful AGNs, providing further support for a common central engine;

f) low-luminosity Seyferts and LINERs share many of the same characteristics in the radio. The transition nuclei detected are those which are the closest, in terms of emission-line diagnostic ratios, to Seyferts and LINERs (Nagar et al., 2002a). Thus at least some transition nuclei are really composite Seyfert/LINER + H II region nuclei, with the nuclear radio luminosity dependent on the Seyfert/LINER component;

g) investigation of all ~ 50 nearby bright galaxies (most of them LLAGNs) with one radio component relatively unambiguously identified with the central engine at sub-parsec resolution, shows that the sub-parsec radio luminosity is correlated with both the estimated mass of the nuclear black hole and the galaxy bulge luminosity. The large scatter in radio luminosity at any given black hole mass may be caused by a range of accretion rates (Eddington ratios $\sim 10^{-1} - 10^{-5}$);

h) about half of all LLAGNs investigated show significant inter-year variability at 15 GHz (2 cm) and 8.4 GHz (3.6 cm) (Nagar et al., 2002a);

i) the nuclear radio luminosity function at 15 GHz of luminous Seyferts, the Palomar sample, and the local group of galaxies extends over the range $10^{15} - 10^{24}$ Watt Hz $^{-1}$, more than five orders of magnitude larger than previous AGN samples. We find $\log \rho \propto -0.78 \times \log L_{15\text{GHz}}$ (where ρ is the space density in Mpc $^{-3}$ mag $^{-1}$), with some evidence for a low luminosity turnover near $\log L_{15\text{GHz}} \sim 19$;

j) within the context of jet models, the primary accretion energy output from LLAGNs with compact radio cores is jet kinetic power; this jet power could dominate the radiated bolometric luminosity by factors of ~ 2 to $> 10^2$. These jets, which are energetically more significant than supernovae in the host galaxy, can potentially deposit sufficient energy into the inner parsecs to significantly slow gas flow into the accretion disk;

k) within the context of jet models, the mass accretion function for Palomar LLAGNs and AGNs has the form $\log \rho \propto -1 \times \dot{M}$. That is, within the Palomar sample, the numerous LLAGNs with low radio luminosity are together accreting the same mass per year as the fewer LLAGNs and AGNs at higher radio luminosity;

l) with increasing Eddington ratio, l_{Edd} , LLAGNs in elliptical galaxies are increasingly radio-loud as measured by the ratio of radio to optical emission-line luminosities;

m) among non-elliptical hosts, LINERs have lower nuclear gas densities, lower Eddington ratios, and are more efficient at launching collimated sub-parsec jets, than low-luminosity Seyferts. We speculate that, by analogy with Galactic black hole candidates, LINERs are in a ‘low/hard’ state while Seyferts are in a ‘high’ state (Sect. 6);

n) high resolution radio imaging is an effective and efficient search technique for finding low luminosity

accreting black holes in LLAGNs.

In short, all evidence points toward the presence of accreting black holes in a large fraction, perhaps all, of LLAGNs. Compact radio jets are an energetically important product of accretion in this low luminosity regime. The radio luminosity function and the jet kinetic powers of these LLAGNs together show that jets are the dominant form of power output from the nuclear accretion and suggest that the jets may input a significant amount of energy into the ISM of their host galaxies.

Acknowledgements. This work was partly funded by the Dutch research organization NWO, through a VENI grant to NN, and by NASA through grants NAG513065 and NAG513557 to the University of Maryland. Parts of this work were completed while NN held a fellowship at Arcetri Observatory, Italy.

8. Appendix: Absorption-line nuclei in the Palomar Sample

The Palomar spectroscopic survey did not detect emission lines in 53 nuclei of the Palomar Sample; upper limits to the H α luminosity in these nuclei are listed in Ho, Filippenko, & Sargent (2003a)⁵. We have searched the literature and VLA archive for high resolution radio observations of these 53 nuclei. The results are listed in Table 3. Only two of the nuclei have AGN-related radio fluxes significantly greater than ~ 1 mJy. NGC 507 (also known as B2 0120+33) has about 100 mJy at 1.4 GHz in larger scale radio lobes but a very weak (~ 1.4 mJy at 5 GHz) radio nucleus (Giovannini et al., 1988); it may be that the AGN is now switched off or in a very low state, which could account for the lack of emission-lines. NGC 4649 has a 1.4 GHz flux of 18 mJy which is distributed in a core plus twin jet structure (Stanger & Warwick, 1986). Another three (possibly 5) of the 53 nuclei have weak (~ 1 mJy) radio nuclei, potentially AGN-related, at 1–5'' resolution (Table 3).

References

- Alonso-Herrero, A., Rieke, M. J., Rieke, G. H., & Shields, J. C. 2000, ApJ, 530, 688
- Anderson, J. M., Ulvestad, J. S., & Ho, L. C. 2004, ApJ, 603, 42
- Antonucci, R. R. J. 1993, ARA&A, 31, 473
- Barth, A. J., Filippenko, A. V., Moran, E. C. 1999, ApJ, 525, 673
- Barth, A. J., Ho, L. C., Filippenko, A. V., & Sargent, W. L. W. 1998, ApJ, 496, 133
- Beasley, A. J., Gordon, D., Peck, A. B., Petrov, L., MacMillan, D. S., Fomalont, E. B., & Ma, C. 2002, ApJS, 141, 13
- Begelman, M. C., Blandford, R. D., & Rees, M. J. 1984, Rev. Mod. Phys., 56, 255
- Bietenholz, M. F., Bartel, N., Rupen, M. P., 2000, ApJ, 532, 895
- Binney, J. 2004a, to appear in MNRAS(astro-ph/0308171)

⁵ Ho, Filippenko, & Sargent (2003a) list 54 nuclei with H α luminosity upper limits; of these, the nucleus of NGC 4494 shows other emission lines and was classified as a (highly uncertain) ‘LINER 2’ by Ho et al. (1997a).

- Binney, J. 2004b, to appear in *Phil Trans Roy Soc* (astro-ph/0407238)
- Binney, J. & Tremaine, S. 1987, ‘Galactic Dynamics’, Princeton, NJ, Princeton University Press, 1987, 747 p.
- Blandford, R. D. 1993, in *Astrophysical Jets*, ed. D. Burgarella, M. Livio, & C. P. O’Dea, (Cambridge: Cambridge Univ. Press), 15
- Braatz, J., Wilson, A. S., & Henkel, C. 1997, *ApJS*, 110, 321
- Carral, P., Turner, J. L., & Ho, P. T. P. 1990, *ApJ*, 362, 434
- Celotti, A. & Fabian, A. C. 1993, *MNRAS*, 264, 228
- Chatterjee, S., Cordes, J. M., Vlemmings, W. H. T., Arzoumanian, Z., Goss, W. M., & Lazio, T. J. W. 2004, *ApJ*, 604, 339
- Colina, L., Alberdi, A., Torrelles, J. M., Panagia, N., & Wilson, A. S. 2001, *ApJ*, 553, L19
- Condon, J. J. 1989, *ApJ*, 338, 13
- Condon, J. J., Cotton, W. D., Greisen, E. W., Yin, Q. F., Perley, R. A., Taylor, G. B., & Broderick, J. J. 1998, *AJ*, 115, 1693
- Condon, J. J., Huang, Z.-P., Yin, Q. F., & Thuan, T. X. 1991, *ApJ*, 378, 65
- Cotton, W. D., Condon, J. J., & Arbizzani, E. 1999, *ApJS*, 125, 409
- Cotton, W. D., Feretti, L., Giovannini, G., Lara, L., & Venturi, T. 1999, *ApJ*, 519, 108
- Crane, P. C., Cowan, J. J., Dickel, J. R., & Roberts, D. A. 1993, *ApJ*, 417, L61
- Dhawan, V., Kellerman, K. I., & Romney, J. D. 1998, *ApJ*, 498, L111
- Di Matteo, T., Carilli, C. L., & Fabian, A. C. 2001, *ApJ*, 547, 731
- Dopita, M. A., & Sutherland, R. S. 1995, *ApJ*, 455, 468
- Emsellem, E., Dejonghe, H., & Bacon, R. 1999, *MNRAS*, 303, 495
- Fabbiano, G., Gioia, I. M., & Trinchieri, G. 1989, *ApJ*, 374, 127
- Falcke, H. & Biermann, P. L. 1999, *A&A*, 342, 49
- Falcke, H., K rding, E., & Markoff, S. 2004, *A&A*, 414, 895
- Falcke, H., Nagar, N. M., Wilson, A. S., & Ulvestad, J. S. 2000, *ApJ*, 542, 197 (Paper II)
- Fender, R. & Belloni, T. 2004, *ARA&A*, 42, 317
- Fender, R. P., Gallo, E., & Jonker, P. G. 2003, *MNRAS*, 343, L99
- Ferrarese, L., & Merritt, D. 2000, *ApJ*, 539, L9
- Filho, M. E., Barthel, P. D., & Ho, L. C. 2000, *ApJS*, 129, 93
- Filho, M. E., Barthel, P. D., & Ho, L. C. 2002, *A&A*, 385, 425
- Filho, M. E., Fraternali, F., Markoff, S., Nagar, N. M., Barthel, P. D., Ho, L. C., & Yuan, F. 2004, *A&A*, 418, 429
- Filippenko, A. V., & Ho, L. C. 2003, *ApJ*, 588, L13
- Filippenko, A. V., & Terlevich, R. 1992, *ApJ*, 397, L79
- Fomalont, E. B., Frey, S., Paragi, Z., Gurvits, L. I., Scott, W. K., Taylor, A. R., Edwards, P. G., & Hirabayashi, H. 2000, *ApJS*, 131, 95
- Fosbury, R. A. E., Mebold, U., Goss, W. M., & Dopita, M. A. 1978, *MNRAS*, 183, 549
- Franceschini, A., Vercellone, S., & Fabian, A. C. 1998, *MNRAS*, 297, 817
- Frank, J., King, A., & Raine, D. 1995, in *Accretion Power in Astrophysics*, 2nd edition, (Cambridge: Cambridge Univ. Press)
- Gebhardt, K., et al. 2000, *ApJ*, 539, L13
- Gebhardt, K., et al. 2003, *ApJ*, 583, 92
- Giovannini, G., Feretti, L., Gregorini, L., & Parma, P. 1988, *A&A*, 199, 73
- Giovannini, G., Cotton, W. D., Feretti, L., Lara, L., & Venturi, T. 2001, *ApJ*, 552, 508
- Heckman, T. M. 1980, *A&A*, 87, 152
- Heckman, T. M., Crane, P. C., & Balick, B. 1980, *A&AS*, 40, 295
- Heckman, T. M., Kauffmann, G., Brinchmann, J., Charlot, S., Tremonti, C., & White, S. D. M. 2004, *ApJ*, 613, 109
- Herrnstein, J. R., Moran, J. M., Greenhill, L. J., Diamond, P. J., Miyoshi, M., Nakai, N., & Inoue, M. 1997, *ApJ*, 475, L17
- Ho, L. C. 2002, *ApJ*, 564, 120
- Ho, L. C. 1999, *ApJ*, 516, 672
- Ho, L. C. et al. 2001, *ApJ*, 549, L51
- Ho, L. C., Filippenko, A. V., & Sargent, W. L. W. 1995, *ApJS*, 98, 477
- Ho, L. C., Filippenko, A. V., & Sargent, W. L. W. 1997a, *ApJS*, 112, 315
- Ho, L. C., Filippenko, A. V., & Sargent, W. L. W. 2003, *ApJ*, 583, 159
- Ho, L. C., Filippenko, A. V., & Sargent, W. L. W., & Peng, C. Y. 1997b, *ApJS*, 112, 391
- Ho, L. C., Terashima, Y., & Ulvestad, J. S. 2003, *ApJ*, 589, 783
- Ho, L. C. & Ulvestad, J. S. 2001, *ApJS*, 133, 77
- Hummel, E. 1980, *A&AS*, 41, 151
- Hummel, E., Fanti, C., Parma, P., & Schilizzi, R. T. 1982, *A&A*, 114, 400
- Hummel, E., van der Hulst, J. M., Keel, W. C., & Kennicutt, R. C. 1987, *A&AS*, 70, 517
- Jones, D. L., & Wehrle, A. E. 1997, *ApJ*, 484, 186
- Jones, D. L., Wehrle, A. E., Piner, B. G., & Meier, D. L. 2001, *ApJ*, 553, 968
- Jones, D. L., Terzian, Y., & Sramek, R. A. 1981, *ApJ*, 246, 28
- Jones, D. L., Wrobel, J. M., & Shaffer, D. B. 1984, *ApJ*, 276, 480
- Junor, W., & Biretta, J. A. 1995, *AJ*, 109, 500
- Karachentsev, I. D., Makarov, D. I., & Huchtmeier, W. K. 1999, *A&AS*, 139, 97
- Kellermann, K. I., Vermeulen, R. C., Zensus, J. A., & Cohen, M. H. 1998, *AJ*, 115, 1295
- Koski, A. T., & Osterbrock, D. E. 1976, *ApJ*, 203, L49
- Krajnovi , D. & Jaffe, W. 2002, *A&A*, 390, 423
- Krichbaum, T. B., et al. 1998, *A&A*, 335, L106
- Kukula, M. J., Ghosh, T., Pedlar, A., & Schilizzi, R. T. 1999, *ApJ*, 518, 117
- Kukula, M. J., Pedlar, A., Baum, S. A., & O’Dea, C. P. 1995, *MNRAS*, 276, 1262
- Laurent-Muehleisen, S. A., Kollgaard, R. I., Ryan, P. J., Feigelson, E. D., Brinkmann, W., & Siebert, J. 1997, *A&AS*, 122, 235
- Lavalley, M., Isobe, T., & Feigelson, E. 1992, in *Astronomical Data Analysis Software and Systems I*, ed. D. Worrall, C. Biemesderfer & J. Barnes, (San Francisco: ASP), Vol. 25, 245 (ASURV)
- Lonsdale, C. J., Lonsdale, C. J., & Smith, H. E. 1992, *ApJ*, 391, 629
- Lonsdale, C. J., Smith, H. J., & Lonsdale, C. J. 1993, *ApJ*, 405, L9
- Lovelace, R. V. E., & Romanova, M. M. 1996, in *Energy Transport in Radio Galaxies*, ed. P. E. Hardee, A. H. Bridle, & J. A. Zensus (San Francisco: ASP), Vol. 100, 25

- Maoz, D., Filippenko, A. V., Ho, L. C., Rix, H.-W., Bahcall, J. N., Schneider, D. P., & Macchetto, F. D. 1995, *ApJ*, 440, 91
- Maoz, D., Koratkar, A., Shields, J. C., Ho, L. C., Filippenko, A. V., & Sternberg, A. 1998, *AJ*, 116, 55
- Marconi, A. & Hunt, L. K. 2003, *ApJ*, 589, L21
- Merloni, A., Heinz, S., & di Matteo, T. 2003, *MNRAS*, 345, 1057
- Merritt, D. & Ferrarese, L. 2001, *MNRAS*, 320, L30
- Meurs, E. J. A. & Wilson, A. S. 1984, *A&A*, 136, 206
- Middelberg, E., et al. 2004, *A&A*, 417, 925
- Mundell, C. G., Wilson, A. S., Ulvestad, J. S., & Roy, A. L. 2000, *ApJ*, 529, 816
- Mundell, C. G., Wrobel, J. M., Pedlar, A., & Gallimore, J. F. 2003, *ApJ*, 583, 192
- Nagar, N. M. 2003, to appear in the proceedings of ‘Multiwavelength AGN Surveys’, Cozumel, December 2003, eds. R. Maiolino & R. Mujica (World Scientific)
- Nagar, N. M., Falcke, H., Wilson, A. S., & Ho, L. C. 2000, *ApJ*, 542, 186 (Paper I)
- Nagar, N. M., Falcke, H., Wilson, A. S., & Ulvestad, J. S. 2002a, *A&A*, 392, 53
- Nagar, N. M., Wilson, A. S., & Falcke, H. 2001, *ApJ*, 559, L87
- Nagar, N. M., Wilson, A. S., Falcke, H., Ulvestad, J. S., & Mundell, C. G. 2002b, *ASP Conf. Ser.* 258: Issues in Unification of Active Galactic Nuclei, 171
- Nagar, N. M., Wilson, A. S., Mulchaey, J. S., & Gallimore, J. F. 1999, *ApJS*, 120, 209
- Napier, P. J., Bagri, D. S., Clark, B. G., Rogers, A. E. E., Romney, J. D., Thompson, A. R., & Walker, R. C. 1994, *Proc. IEEE*, 82, 658
- Narayan, R., Mahadevan, R., & Quataert, E. 1998, in *The Theory of Black Hole Accretion Discs*, ed. M. A. Abramowicz, G. Björnsson, & J. E. Pringle (Cambridge: Cambridge Univ. Press), 148
- Narayan, R., Igumenshchev, I. V., & Abramowicz, M. A. 2000, *ApJ*, 539, 798
- Neff, S. G., & Ulvestad, J. S. 2000, *AJ*, 120, 670
- Osterbrock, D. E. 1981, *ApJ*, 249, 462
- Osterbrock, D. E. 1989, *Astrophysics of Gaseous Nebulae and Active Galactic Nuclei* (Mill Valley, CA: Univ. Sci. Books)
- Ostriker, J. P., & Ciotti, L. 2004, to appear in *Phil Trans Roy Soc (astro-ph/0407234)*
- Owen, F. N., Eilek, J. A., & Kassim, N. E. 2000, *ApJ*, 543, 611
- Pellegrini, S. & Ciotti, L. 1998, *A&A*, 333, 433
- Pringle, J. E. 1993, in *Astrophysical Jets*, ed. D. Burgerella, M. Livio, & C. P. O’Dea, (Cambridge: Cambridge Univ. Press), 1
- Rawlings, S. & Saunders, R. 1991, *Nature*, 349, 138
- Rees, M. J., Phinney, E. S., Begelman, M. C., & Blandford, R. D. 1982, *Nature*, 295, 1
- Richstone, D., et al. 1998, *Nature*, 395A, 14
- Sadler, E. M., Jenkins, C. R., & Kotanyi, C. G. 1989, *MNRAS*, 240, 591
- Sadler, E. M., Slee, O. B., Reynolds, J. E., & Roy, A. L. 1995, *MNRAS*, 276, 1373
- Sandage, A., Tammann, G. A., & Yahil, A. 1979, *ApJ*, 232, 352
- Sanghera, H. S., Saikia, D. J., Luedke, E., Spencer, R. E., Foulsham, P. A., Akujor, C. E., & Tzioumis, A. K. 1995, *A&A*, 295, 629
- Schilizzi, R. T., Fanti, C., Fanti, R., & Parma, P. 1983, *A&A*, 126, 412
- Shields, J. C. 1992, *ApJ*, 399, L27
- Sjouwerman, L., Mioduszewski, A., & Greisen, T. 2004, in preparation
- Slee, O. B., Sadler, E. M., Reynolds, J. E., & Ekers, R. D. 1994, *MNRAS*, 269, 928
- Smith, H. E., Lonsdale, C. J., & Lonsdale, C. J. 1998, *ApJ*, 492, 137
- Soltan, A. 1982, *MNRAS*, 200, 115
- Stanger, V. J. & Warwick, R. S. 1986, *MNRAS*, 220, 363
- Stoughton, C., et al. 2002, *AJ*, 123, 485
- Terashima, Y., Ho, L. C., & Ptak, A. F. 2000, *ApJ*, 539, 161
- Terashima, Y. & Wilson, A. S. 2003, *ApJ*, 583, 145
- Terlevich, R., & Melnick J. 1985, *MNRAS*, 213, 841
- Terlevich, R., Tenorio-Tagle, G., Franco, J., & Melnick, J. 1995, *MNRAS*, 272, 198
- Thompson, A. R., Clark, B. G., Wade, C. M., & Napier, P. J. 1980, *ApJS*, 44, 151
- Tremaine, S., et al. 2002, *ApJ*, 574, 740
- Trotter, A. S., Greenhill, L. J., Moran, J. M., Reid, M. J., Irwin, J. A., & Lo, K. 1998, *ApJ*, 495, 740
- Ulvestad, J. S. & Ho, L. C. 2001, *ApJ*, 558, 561
- Ulvestad, J. S. & Ho, L. C. 2001, *ApJ*, 562, L133
- Ulvestad, J. S., Roy, A. L., Colbert, E. J. M., & Wilson, A. S. 1998, *ApJ*, 496, 196
- Ulvestad, J. S., & Wilson, A. S. 1989, *ApJ*, 343, 659
- Ulvestad, J. S., Wrobel, J. M., Roy, A. L., Wilson, A. S., Falcke, H., & Krichbaum, T. P. 1999, *ApJ*, 517, L81
- Woo, J., & Urry, C. M. 2002, *ApJ*, 579, 530
- Venturi, T., Giovannini, G., Feretti, L., Comoretto, G., & Wehrle, A. E. 1993, *ApJ*, 408, 81
- van den Bergh, S. & McClure, R. D. 1994, *ApJ*, 425, 205
- Verdoes Kleijn, G. A., Baum, S. A., de Zeeuw, P. T., & O’Dea, C. P. 2002, *AJ*, 123, 1334
- Vila, M. B., Pedlar, A., Davies, R. D., Hummel, E. & Axon, D. J. 1990, *MNRAS*, 242, 379
- Walker, R. C., Dhawan, V., Romney, J. D., Kellermann, K. I., & Vermeulen, R. C. 2000, *ApJ*, 530, 233
- White, R. L., Becker, R. H., Helfand, D. J., & Gregg, M. D. 1997, *ApJ*, 475, 479 (FIRST)
- Wrobel, J. M. 2000, *ApJ*, 531, 716
- Wrobel, J. M., Fassnacht, C. D., & Ho, L. C. 2001, *ApJ*, 553, L23
- Wrobel, J. M., & Heeschen, D. S. 1984, *ApJ*, 287, 41
- Wrobel, J. M., & Heeschen, D. S. 1991, *AJ*, 101, 148
- Wrobel, J. M., Machalski, J., & Condon, J. J., in preparation
- Wrobel, J. M., Walker, R. C., & Bridle, A. H. 1996, in *Extragalactic radio sources: proc. of the 175th Symposium of the IAU*, ed. R. D. Ekers, C. Fanti, & L. Padrielli (Kluwer Academic Publishers), 131
- Xu, C., Baum, S. A., O’Dea, C. P., Wrobel, J. M., & Condon, J. J. 2000, *AJ*, 120, 2950
- Zensus, J. A. 1997, *ARA&A*, 35, 607
- Zirbel, E. L., & Baum, S. A. 1995, *ApJ*, 448, 521

Fig. 8.A
plot
of
Jet
Power
(we
use
the
'min-
i-
mum
jet
power',
 Q_{jet} ,
de-
rived
from
the
the
*nu-
clear*
ra-
dio
lu-
mi-
nos-
ity;see
text)
ver-
sus
the
Narrow
Line
Region
(NLR)
lu-
mi-
nos-
ity
(de-
rived
from
the
[O III]
lu-
mi-
nos-
ity;see
text)
for
radio-
detected
nu-
clei
in
the
Palomar
Sample
(cir-
cles).
Filled
cir-
cles
are
used
for
el-
i-

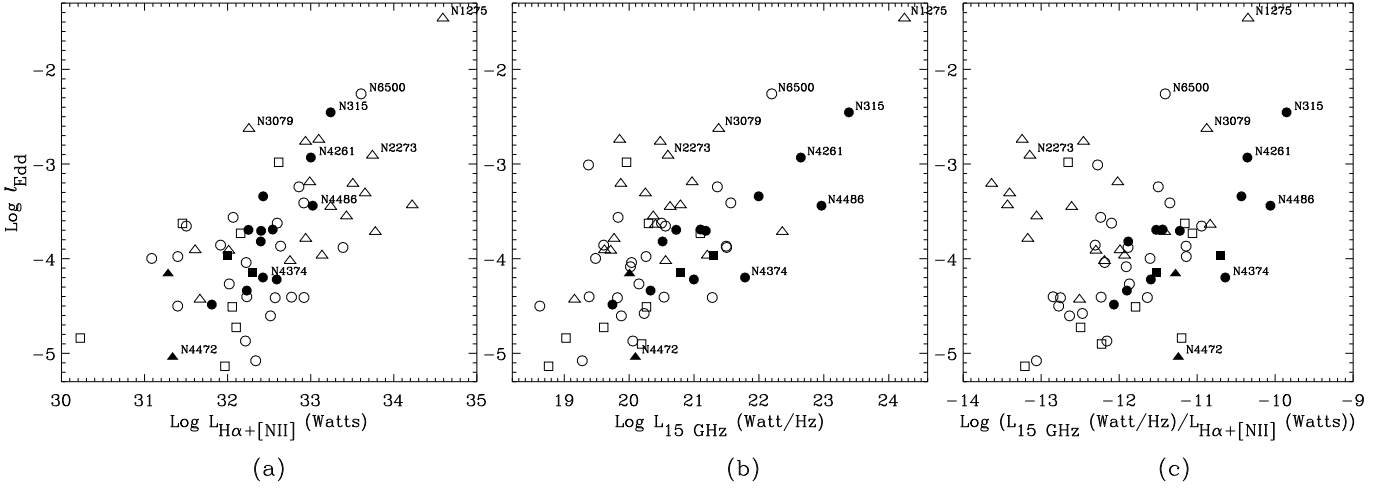


Fig. 10. Plots of the ‘minimum jet power’ as a fraction of Eddington luminosity (equivalent to the Eddington ratio, l_{Edd} , if the jet power dominates the emitted accretion energy) versus (a) the nuclear $\text{H}\alpha + [\text{N II}] \lambda\lambda 6548, 6583$ luminosity, (b) the 15 GHz nuclear (150 mas resolution) radio luminosity, and (c) ratio of the above two quantities, for all radio-detected LLAGNs and AGNs in the Palomar sample. Seyferts are plotted as triangles, LINERs as circles, and transition nuclei as squares. Filled symbols are used for elliptical galaxies.

TABLE 3: RADIO FLUXES FOR PALOMAR ABSORPTION-LINE NUCLEI

Name	$L_{\text{H}\alpha}$ (erg/s)	S_{radio} (mJy)	Ref.	Name	$L_{\text{H}\alpha}$ (erg/s)	S_{radio} (mJy)	Ref.
NGC 147	<35.19	<1.5	NVSS	NGC 4382	<38.10	<0.5	WH91
NGC 205	<34.79	1.0	N04	NGC 4406	<37.82	<0.5, 0.6	WH91, KJ02
NGC 221	<36.19	<0.03	T03	NGC 4417	<37.88	<0.5	WH91
NGC 507	<38.74	1.4–100	G88, NVSS	NGC 4421	<37.37	≤1.5 mJy	NVSS
NGC 628	<36.69	NGC 4442	<37.98	<0.5	WH91
NGC 821	<38.13	<0.5, <1.5	WH91, N04	NGC 4461	<37.92	<0.5	WH91
NGC 1023	<37.82	<1.5	N04	NGC 4473	<38.06	<2.0	WH91
NGC 2300	<38.19	0.7	F89	NGC 4478	<37.67	<5.0	WH91
NGC 2549	<38.05	<0.1	KJ02	NGC 4503	<37.67	<0.5	WH91
NGC 2634	<38.07	NGC 4564	<37.83	<0.5	WH91
NGC 2775	<37.94	<1.5	H87	NGC 4570	<38.02	<0.5	WH91
NGC 2950	<38.42	<1.5	NVSS	NGC 4578	<37.58	<0.5	WH91
NGC 3115	<37.80	<0.4	F89	NGC 4608	<37.65	<1.0	WH91
NGC 3384	<37.56	<0.5	WH91	NGC 4612	<37.63	<0.5	WH91
NGC 3610	<38.55	<0.5, 1.2	WH91, KJ02	NGC 4621	<37.99	<0.5	WH91
NGC 3613	<38.32	<0.5	WH91	NGC 4638	<37.93	<0.5	WH91
NGC 3640	<38.18	<0.5	WH91	NGC 4648	<38.41	<0.5	WH91
NGC 3838	<38.12	<1.5	NVSS	NGC 4665	<37.93	<0.4	F89
NGC 4026	<38.10	1.4	WH91	NGC 4649	<37.73	~18 mJy	SW86
NGC 4179	<38.45	<0.5	WH91	NGC 4754	<38.01	<0.5	WH91
NGC 4251	<37.74	<0.5	WH91	NGC 4914	<38.84	<1.0	FIRST
NGC 4267	<37.88	<0.5	WH91	NGC 5473	<38.39	<0.5	WH91
NGC 4291	<38.38	<0.4	WH91, F89	NGC 5576	<38.49	<0.1	WH91, KJ02
NGC 4339	<38.02	<0.5	WH91	NGC 6654	<38.11	<1.5	NVSS
NGC 4365	<37.98	<0.1	WH91, KJ02	NGC 7332	<38.03	<1.5	N04
NGC 4371	<37.61	<0.5	WH91	NGC 7457	<37.24	1.1	N04
NGC 4379	<37.63	<0.5	WH91

^aThis table lists all 53 nuclei without detected emission-lines in the Palomar Sample (Ho et al. 2003). The columns list the galaxy name (in bold if the nucleus has radio flux ≥ 1 mJy), upper limit to the $\text{H}\alpha$ luminosity (from Ho et al. 2003), the VLA radio flux (at the highest resolution found; multiple values are listed when significantly different data are available), and reference(s) for the radio flux.

^bThe reference codes are: **F89**: Fabbiano et al. 1989, 5 GHz, $\sim 0''.6$ or $\sim 5''$ resolution; **FIRST**: VLA FIRST survey (White et al. 1997), 1.4 GHz, $5''$ resolution; **H87**: Hummel et al. (1987), 1.4 GHz, $1''.5$ resolution; **KJ02**: Krajnović & Jaffe (2002), 8.4 GHz, $2''.5$ resolution; **N04**: this work, 15 GHz, 150 mas resolution; **NVSS**: VLA NVSS survey (Condon et al. 1998), 1.4 GHz, $45''$ resolution; **SW86**: Stanger & Warwick (1986), 1.4 GHz and 5 GHz imaging with resolution $4''$ and $1''.2$, respectively; **WH91**: Wrobel & Heeschen (1991), 5 GHz, $5''$ resolution.

^c**Notes**: NGC 507 (B2 0120+33) has twin radio lobes and a weak 1.4 mJy core; NGC 4406 was not detected by WH91, but detected by KJ02; NGC 4649 has a core plus twin jet structure.

TABLE 1
HIGH-RESOLUTION 15 GHz VLA IMAGING OF PALOMAR SAMPLE AGN AND LLAGN

Name	Activity Type	T	Dist. (Mpc)	R.A. (J2000)	Dec. (J2000)	Δ (")	S_{peak} (mJy/beam)	S_{tot} (mJy)	$\text{Log } L_{15\text{GHz}}^{\text{peak}}$ (W Hz^{-1})	Com.
(1)	(2)	(3)	(4)	(5)	(6)	(7)	(8)	(9)	(10)	(11)
IC 239	L2::	6.0	16.8	< 0.9	< 19.48	
IC 356	T2	2.0	18.1	< 1.0	< 19.59	4
IC 520	T2:	2.0	47.0	< 1.0	< 20.42	4
IC 1727	T2/L2	9.0	8.2	< 0.9	< 18.86	
NGC 185	S2	-5.0	0.7	< 1.1	< 16.81	
NGC 266	L1.9	2.0	62.4	00 49 47.819	32 16 39.71	2.0	4.1	4.1	21.28	
NGC 315	L1.9	-4.0	65.8	^a	^a	...	470.0	...	23.39	9
NGC 404	L2	-3.0	2.4	< 1.3	< 17.95	
NGC 410	T2:	-4.0	70.6	< 1.0	< 20.78	4
NGC 428	L2/T2:	9.0	14.9	< 0.9	< 19.38	
NGC 474	L2::	-2.0	32.5	< 1.5	< 20.28	
NGC 488	T2::	3.0	29.3	< 1.0	< 20.01	4
NGC 521	T2/H:	4.0	67.0	< 1.0	< 20.73	4
NGC 524	T2:	-1.0	32.1	^a	^a	...	1.5	1.5	20.27	3
NGC 660	T2/H:	1.0	11.8	< 0.9	< 19.18	
NGC 676	S2:	0.0	19.5	< 1.5	< 19.83	
NGC 718	L2	1.0	21.4	< 1.5	< 19.91	
NGC 777	S2/L2::	-5.0	66.5	< 1.5	< 20.90	
NGC 841	L1.9:	2.1	59.5	< 1.5	< 20.80	
NGC 1055	T2/L2::	3.0	12.6	< 1.8	< 19.53	
NGC 1058	S2	5.0	9.1	< 0.9	< 18.95	
NGC 1167	S2	-3.0	65.3	03 01 42.347	35 12 20.07	1.2	44.9	248.7	22.36	
NGC 1169	L2	3.0	33.7	< 1.5	< 20.31	
NGC 1275	S1.5	10.0	70.1	^a	^a	...	2970.0	...	24.24	10
NGC 1961	L2	5.0	53.1	< 1.5	< 20.70	
NGC 2273	S2	0.5	28.4	06 50 08.652	60 50 44.95	0.8	4.1	5.1	20.60	
NGC 2336	L2/S2	4.0	33.9	< 1.5	< 20.31	
NGC 2541	T2/H:	6.0	10.6	< 1.0	< 19.13	
NGC 2655	S2	0.0	24.4	08 55 38.071	78 13 23.77	2.8	6.0	6.0	20.63	
NGC 2681	L1.9	0.0	13.3	< 1.4	< 19.48	
NGC 2683	L2/S2	3.0	5.7	< 0.9	< 18.54	
NGC 2685	S2/T2:	-1.0	16.2	< 0.9	< 19.45	
NGC 2768	L2	-5.0	23.7	09 11 37.413	60 02 14.86	0.9	7.9	8.2	20.73	
NGC 2787	L1.9	-1.0	13.0	09 19 18.607	69 12 11.64	1.6	7.0	7.0	20.15	
NGC 2832	L2::	-4.0	91.6	< 1.5	< 21.18	
NGC 2841	L2	3.0	12.0	09 22 02.678	50 58 35.70	7.4	1.1	2.1	19.28	
NGC 2859	T2:	-1.0	25.4	< 1.0	< 19.89	4
NGC 2911	L2	-2.0	42.2	09 33 46.108	10 09 08.82	0.5	17.3	17.7	21.57	
NGC 2985	T1.9	2.0	22.4	< 1.0	< 19.78	4
NGC 3031	S1.5	2.0	3.6	09 55 33.175	69 03 55.06	6.4	164.1	164.8	20.41	
NGC 3079	S2	7.0	20.4	^a	^a	...	48.0	59.0	21.38	7
NGC 3147	S2	4.0	40.9	10 16 53.648	73 24 02.69	1.6	8.0	8.1	21.20	
NGC 3166	L2	0.0	22.0	< 1.5	< 19.94	
NGC 3169	L2	1.0	19.7	10 14 15.052	03 27 57.86	3.7	6.8	6.8	20.50	
NGC 3190	L2	1.0	22.4	10 18 06.005	21 49 54.55	5.8	1.1	0.8	19.82	
NGC 3193	L2:	-5.0	23.2	< 1.5	< 19.99	
NGC 3226	L1.9	-5.0	23.4	10 23 27.014	19 53 54.59	0.9	5.0	5.4	20.52	
NGC 3227	S1.5	1.0	20.6	10 23 30.579	19 51 54.19	0.8	3.5	4.7	20.25	
NGC 3245	T2:	-2.0	22.2	< 1.0	< 19.77	4
NGC 3254	S2	4.0	23.6	< 1.5	< 20.00	
NGC 3301	L2	0.0	23.3	< 1.5	< 19.99	
NGC 3368	L2	2.0	8.1	< 1.0	< 18.89	
NGC 3379	L2/T2::	-5.0	8.1	< 1.0	< 18.89	
NGC 3414	L2	-2.0	24.9	10 51 16.210	27 58 30.31	0.3	2.3	2.4	20.23	
NGC 3433	L2/T2::	5.0	39.5	< 1.5	< 20.45	
NGC 3486	S2	5.0	7.4	< 1.0	< 18.82	
NGC 3489	T2/S2	-1.0	6.4	< 1.0	< 18.69	
NGC 3507	L2	3.0	19.8	< 1.5	< 19.85	
NGC 3516	S1.2	-2.0	38.9	^a	^a	...	1.3	1.3	20.37	8
NGC 3607	L2	-2.0	19.9	11 16 54.668	18 03 06.43	1.2	1.6	1.4	19.88	
NGC 3608	L2/S2:	-5.0	23.4	< 1.5	< 19.99	
NGC 3623	L2:	1.0	7.3	< 0.9	< 18.76	
NGC 3626	L2:	-1.0	26.3	< 1.5	< 20.09	
NGC 3627	T2/S2	3.0	6.6	11 20 15.008	12 59 29.76	8.2	1.1	2.9	18.76	
NGC 3628	T2	3.0	7.7	11 20 17.016	13 35 20.04	6.5	1.5	2.2	19.03	

TABLE 1—*Continued*

Name	Activity Type	T	Dist. (Mpc)	R.A. (J2000)	Dec. (J2000)	Δ (")	S_{peak} (mJy/beam)	S_{tot} (mJy)	$\text{Log } L_{15\text{GHz}}^{\text{peak}}$ (W Hz^{-1})	Com.
(1)	(2)	(3)	(4)	(5)	(6)	(7)	(8)	(9)	(10)	(11)
NGC 3642	L1.9	4.0	27.5	< 1.3	< 20.06	
NGC 3675	T2	3.0	12.8	< 1.0	< 19.29	
NGC 3681	T2:	4.0	24.2	< 1.0	< 19.85	4
NGC 3692	T2	3.0	29.8	< 1.2	< 20.09	
NGC 3705	T2	2.0	17.0	< 1.2	< 19.61	
NGC 3718	L1.9	1.0	17.0	11 32 34.856	53 04 04.51	2.0	10.5	10.8	20.56	
NGC 3735	S2:	5.0	41.0	< 1.5	< 20.48	
NGC 3780	L2::	5.0	37.2	11 39 22.267	56 16 10.17	4.2	1.1	1.0	20.26	
NGC 3898	T2	2.0	21.9	< 1.0	< 19.76	4
NGC 3900	L2:	-1.0	29.4	< 1.5	< 20.19	
NGC 3917	T2:	6.0	17.0	< 1.2	< 19.63	
NGC 3941	S2:	-2.0	18.9	< 1.1	< 19.67	
NGC 3945	L2	-1.0	22.5	11 53 13.609	60 40 32.12	1.4	1.8	2.1	20.04	
NGC 3953	T2	4.0	17.0	< 1.3	< 19.64	
NGC 3976	S2:	3.0	37.7	< 1.5	< 20.41	
NGC 3982	S1.9	3.0	17.0	< 1.0	< 19.54	
NGC 3992	T2:	4.0	17.0	< 1.3	< 19.64	
NGC 3998	L1.9	-2.0	21.6	^a	^a	...	57.0	57.0	21.50	12
NGC 4013	T2	3.0	17.0	< 1.0	< 19.54	
NGC 4036	L1.9	-3.0	24.6	12 01 26.433	61 53 45.91	2.6	...	< 1.5	< 20.04	2
NGC 4051	S1.2	4.0	17.0	< 1.0	< 19.54	
NGC 4111	L2	-1.0	17.0	< 1.3	< 19.64	
NGC 4125	T2	-5.0	24.2	< 1.0	< 19.85	4
NGC 4138	S1.9	-1.0	17.0	12 09 29.800	43 41 06.89	1.2	1.5	1.3	19.71	
NGC 4143	L1.9	-2.0	17.0	12 09 36.067	42 32 03.05	1.6	3.3	3.3	20.06	
NGC 4145	T2:	7.0	20.7	< 1.3	< 19.81	
NGC 4150	T2	-2.0	9.7	< 1.0	< 19.05	
NGC 4151	S1.5	2.0	20.3	^a	^a	...	12.5	17.6	20.79	7
NGC 4168	S1.9:	-5.0	16.8	12 12 17.270	13 12 18.75	1.0	3.0	3.1	20.01	
NGC 4169	S2	-2.0	50.4	12 12 19.091	29 10 45.03	2.3	1.2	1.0	20.56	
NGC 4192	T2	2.0	16.8	12 13 48.269	14 53 59.11	1.8	...	< 1.3	< 19.64	2
NGC 4203	L1.9	-3.0	9.7	12 15 05.056	33 11 50.25	1.1	9.5	9.5	20.03	
NGC 4216	T2	3.0	16.8	12 15 54.375	13 08 58.13	2.2	1.2	1.3	19.61	
NGC 4220	T2	-1.0	17.0	< 1.4	< 19.70	
NGC 4258	S1.9	4.0	6.8	12 18 57.505	47 18 14.32	0.4	2.6	3.0	19.16	
NGC 4261	L2	-5.0	35.1	^a	^a	...	300.0	...	22.65	11
NGC 4278	L1.9	-5.0	9.7	12 20 06.824	29 16 50.74	1.7	88.3	89.7	21.00	
NGC 4281	T2::	-1.0	35.1	< 1.0	< 20.17	4
NGC 4293	L2	0.0	17.0	12 21 12.813	18 22 56.75	5.6	0.7	1.4	19.38	6
NGC 4314	L2	1.0	9.7	< 1.0	< 19.05	
NGC 4321	T2	4.0	16.8	< 0.9	< 19.48	
NGC 4324	T2::	-1.0	35.1	< 1.0	< 20.17	4
NGC 4346	L2::	-2.0	17.0	< 1.0	< 19.54	
NGC 4350	T2::	-2.0	16.8	< 0.9	< 19.48	
NGC 4374	L2	-5.0	16.8	12 25 03.745	12 53 13.19	3.2	180.7	183.7	21.79	
NGC 4378	S2	1.0	35.1	< 1.5	< 20.34	
NGC 4388	S1.9	3.0	16.8	12 25 46.783	12 39 43.79	2.2	2.2	3.7	19.87	
NGC 4394	L2	3.0	16.8	< 0.9	< 19.48	
NGC 4395	S1.8	9.0	3.6	< 0.9	< 18.14	
NGC 4414	T2:	5.0	9.7	< 0.9	< 19.01	
NGC 4419	T2	1.0	16.8	12 26 56.452	15 02 50.80	2.8	2.7	3.6	19.96	
NGC 4429	T2	-1.0	16.8	< 1.1	< 19.57	
NGC 4435	T2/H:	-2.0	16.8	< 1.1	< 19.57	
NGC 4438	L1.9	0.0	16.8	< 0.9	< 19.48	
NGC 4450	L1.9	2.0	16.8	12 28 29.592	17 05 06.01	1.4	2.0	2.7	19.83	
NGC 4457	L2	0.0	17.4	< 1.0	< 19.56	
NGC 4459	T2:	-1.0	16.8	< 1.0	< 19.53	
NGC 4472	S2::	-5.0	16.8	12 29 46.761	08 00 01.68	1.8	3.7	4.1	20.10	
NGC 4477	S2	-2.0	16.8	< 1.0	< 19.53	
NGC 4486	L2	-4.0	16.8	12 30 49.422	12 23 28.03	3.1	2725.7	2835.7	22.96	
NGC 4494	L2::	-5.0	9.7	< 0.8	< 18.95	
NGC 4501	S2	3.0	16.8	< 1.1	< 19.57	
NGC 4527	T2	4.0	13.5	< 1.1	< 19.38	
NGC 4548	L2	3.0	16.8	12 35 26.448	14 29 46.71	2.5	1.2	1.2	19.61	
NGC 4550	L2	-1.5	16.8	12 35 30.078	12 13 18.63	10.8	0.7	0.7	19.37	6

TABLE 1—*Continued*

Name	Activity Type	T	Dist. (Mpc)	R.A. (J2000)	Dec. (J2000)	Δ (")	S_{peak} (mJy/beam)	S_{tot} (mJy)	$\text{Log } L_{15\text{GHz}}^{\text{peak}}$ (W Hz^{-1})	Com.
(1)	(2)	(3)	(4)	(5)	(6)	(7)	(8)	(9)	(10)	(11)
NGC 4552	T2:	-5.0	16.8	12 35 39.807	12 33 22.82	2.8	58.1	58.6	21.29	
NGC 4565	S1.9	3.0	9.7	12 36 20.778	25 59 15.65	4.5	3.7	3.7	19.62	
NGC 4569	T2	2.0	16.8	< 1.1	< 19.57	
NGC 4579	S1.9/L1.9	3.0	16.8	12 37 43.523	11 49 05.48	3.1	27.6	28.3	20.97	
NGC 4589	L2	-5.0	30.0	12 37 24.986	74 11 30.89	1.0	11.7	11.9	21.10	
NGC 4596	L2::	-1.0	16.8	< 1.1	< 19.57	
NGC 4636	L1.9	-5.0	17.0	12 42 49.831	02 41 15.98	2.6	1.6	1.9	19.74	
NGC 4639	S1.0	4.0	16.8	< 1.1	< 19.57	
NGC 4643	T2	0.0	25.7	< 1.0	< 19.90	4
NGC 4651	L2	5.0	16.8	< 1.1	< 19.57	
NGC 4698	S2	2.0	16.8	< 1.0	< 19.53	
NGC 4713	T2	7.0	17.9	< 1.1	< 19.63	
NGC 4725	S2:	2.0	12.4	< 0.9	< 19.22	
NGC 4736	L2	2.0	4.3	12 50 53.070	41 07 12.95	6.2	1.9	1.7	18.62	
NGC 4750	L1.9	2.0	26.1	< 1.5	< 20.09	
NGC 4762	L2:	-2.0	16.8	12 52 55.903	11 13 46.60	2.9	0.9	1.3	19.48	6
NGC 4772	L1.9	1.0	16.3	12 53 29.162	02 10 06.16	2.5	3.3	3.4	20.02	
NGC 4826	T2	2.0	4.1	< 0.9	< 18.26	
NGC 4866	L2	-1.0	16.0	< 1.1	< 19.53	
NGC 5005	L1.9	4.0	21.3	< 1.1	< 19.78	
NGC 5012	T2	5.0	40.4	< 1.0	< 20.29	4
NGC 5033	S1.5	5.0	18.7	13 13 27.471	36 35 37.93	1.8	1.4	1.4	19.77	
NGC 5055	T2	4.0	7.2	< 1.1	< 18.83	
NGC 5194	S2	4.0	7.7	< 1.1	< 18.89	
NGC 5195	L2:	10.0	9.3	< 1.1	< 19.06	
NGC 5273	S1.5	-2.0	21.3	< 1.1	< 19.78	
NGC 5297	L2	4.5	37.8	< 1.5	< 20.41	
NGC 5322	L2::	-5.0	31.6	13 49 15.265	60 11 25.93	0.0	12.7	12.7	21.18	
NGC 5353	L2/T2:	-2.0	37.8	13 53 26.694	40 16 58.87	0.6	18.3	18.7	21.50	
NGC 5354	T2/L2:	-2.0	32.8	^a	^a	...	9.7	9.7	21.10	3
NGC 5363	L2	10.0	22.4	13 56 07.214	05 15 17.25	2.5	38.1	40.7	21.36	
NGC 5371	L2	4.0	37.8	< 1.5	< 20.41	
NGC 5377	L2	1.0	31.0	13 56 16.834	47 14 06.27	0.5	3.0	3.1	20.54	
NGC 5395	S2/L2	3.0	46.7	< 1.5	< 20.59	
NGC 5448	L2	1.0	32.6	< 1.5	< 20.28	
NGC 5485	L2:	-2.0	32.8	< 1.5	< 20.29	
NGC 5566	L2	2.0	26.4	< 1.1	< 19.96	
NGC 5631	S2/L2:	-2.0	32.7	< 1.5	< 20.28	
NGC 5656	T2::	2.0	42.6	< 1.0	< 20.34	4
NGC 5678	T2	3.0	35.6	< 1.0	< 20.18	4
NGC 5701	T2:	0.0	26.1	< 1.1	< 19.95	
NGC 5746	T2	3.0	29.4	< 1.0	< 20.01	4
NGC 5813	L2:	-5.0	28.5	15 01 11.228	01 42 07.14	1.6	2.2	2.4	20.33	5
NGC 5838	T2::	-3.0	28.5	^a	^a	...	1.6	1.6	20.19	3
NGC 5846	T2:	-5.0	28.5	^a	^a	...	6.3	6.3	20.79	3
NGC 5850	L2	3.0	28.5	1
NGC 5866	T2	-1.0	15.3	15 06 29.500	55 45 47.58	0.4	7.1	7.5	20.30	
NGC 5879	T2/L2	4.0	16.8	< 1.1	< 19.57	
NGC 5921	T2	4.0	25.2	< 1.0	< 19.88	4
NGC 5970	L2/T2:	5.0	31.6	1
NGC 5982	L2::	-5.0	38.7	1
NGC 5985	L2	3.0	39.2	1
NGC 6340	L2	0.0	22.0	< 1.5	< 19.94	
NGC 6384	T2	4.0	26.6	< 1.0	< 19.93	4
NGC 6482	T2/S2::	-5.0	52.3	< 1.0	< 20.52	4
NGC 6500	L2	1.7	39.7	17 55 59.782	18 20 17.65	1.7	83.5	85.0	22.20	
NGC 6503	T2/S2:	6.0	6.1	< 1.0	< 18.65	
NGC 6703	L2::	-2.5	35.9	< 1.5	< 20.36	
NGC 6951	S2	4.0	24.1	< 1.5	< 20.02	
NGC 7177	T2	3.0	18.2	< 1.1	< 19.64	
NGC 7217	L2	2.0	16.0	22 07 52.395	31 21 33.65	2.9	...	< 0.6	< 19.23	2
NGC 7331	T2	3.0	14.3	< 1.1	< 19.43	
NGC 7479	S1.9	5.0	32.4	23 04 56.632	12 19 22.65	1.0	2.4	2.5	20.48	
NGC 7626	L2::	-5.0	45.6	23 20 42.538	08 13 00.98	2.9	39.8	40.0	22.00	
NGC 7742	T2/L2	3.0	22.2	< 1.1	< 19.81	

TABLE 1—*Continued*

Name	Activity Type	T	Dist. (Mpc)	R.A. (J2000)	Dec. (J2000)	Δ (")	S_{peak} (mJy/beam)	S_{tot} (mJy)	$\text{Log } L_{15\text{GHz}}^{\text{peak}}$ (W Hz^{-1})	Com.
(1)	(2)	(3)	(4)	(5)	(6)	(7)	(8)	(9)	(10)	(11)
NGC 7743	S2	−1.0	24.4	23 44 21.364	09 56 03.84	1.1	1.0	1.5	19.85	
NGC 7814	L2::	2.0	15.1	< 1.1	< 19.48	

Note. — This table lists all AGNs and low-luminosity AGNs – i.e. all Seyferts, LINERs, and transition nuclei in the Palomar spectroscopic sample of nearby bright galaxies. All appropriate columns are listed for radio data from Nagar et al. 2000, Nagar et al. 2002, and this paper. For sources taken from the literature, not all columns are listed; the listed and the remaining data can be accessed from the reference listed in col 11.

Note. — Columns are: (1) galaxy name; (2) nuclear activity type as given by H97a. ‘L’ represents LINER, ‘S’ represents Seyfert, ‘H’ represents an H II region type spectrum, and ‘T’ represents objects with transitional ‘L’ + ‘H’ spectra. ‘2’ implies that no broad $\text{H}\alpha$ is detected, ‘1.9’ implies that broad $\text{H}\alpha$ is present, but not broad $\text{H}\beta$, and ‘1.0’ or ‘1.5’ implies that both broad $\text{H}\alpha$ and broad $\text{H}\beta$ are detected, with the specific type depending on the ratio of the flux in $[\text{O III}] \lambda 5007$ to the flux in broad + narrow $\text{H}\beta$ (e.g. Osterbrock 1981). The ‘:’ and ‘::’ symbols represent uncertain, and highly uncertain, classifications, respectively; (3) Hubble morphological parameter T as listed in H97a; (4) distance in Mpc to galaxy, as listed in H97a; (5) and (6) 15 GHz radio position (J2000), from our 15 GHz A-configuration VLA maps, unless otherwise mentioned. Positions in Nagar et al. (2000,2002) were reported in equinox B1950. Here we have precessed the B1950 positions to J2000 using the SCHED software (see text). For entries marked ‘a’ the position can be found in the reference listed in column 11; (7) offset, in arcsec, between the 15 GHz radio position and the position of the galaxy optical nucleus listed in Cotton et al. 1999; (8) and (9) peak and total flux-density, obtained by fitting a single Gaussian (with peak flux-density, major and minor axes as free parameters) to the radio nuclear source in our maps; (10) logarithm of the radio luminosity (derived from the *peak* radio flux); (11) Comments as listed below.

Note. — Comments: 1. these are the only 4 LLAGNs in the sample which remain unobserved at high resolution; 2. radio position from VLA D-configuration maps (Nagar et al. 2000); 3. 15 GHz flux estimated from data in Filho et al. (2004); 4. not detected in $\sim 1''.5$ resolution 8.4 GHz VLA maps (Filho et al. 2002, 2004) and thus taken to be < 1 mJy at 15 GHz; 5. 15 GHz flux and position from Birkinshaw et al. (priv. communication); derived from $0''.4$ resolution 5 GHz VLA imaging; 6. this is a tentative ($< 5\sigma$) detection; 7. 15 GHz flux from Carral et al. (1990); 8. 15 GHz flux estimated from data in Ulvestad & Wilson (1989); 9. 15 GHz flux estimated from data in Venturi et al.(1993); 10. 15 GHz flux estimated from data in Dhawan et al. (1998); 11. 15 GHz flux estimated from data in Jones & Wehrle (1997); 12. 15 GHz flux estimated from data in Wrobel & Heeschen (1984).

TABLE 2: VLBI OBSERVATIONS OF PALOMAR SAMPLE LLAGNs AND AGNs

Name	Act.	T	Dist.	L _{Hα}	R.A.	Dec.	S _{peak} ^{core}	S _{tot} ^{core}	S _{tot} ^{mas}	Lg L _{peak} ^{core}	Size	PA	Beam	BPA	Lg T _b	Scale	Com.
(1)	Type	(3)	(Mpc)	(5)	(J2000)	(J2000)	(mJy)	(mJy)	(mJy)	(W/Hz)	(mas)	(°)	(mas)	(deg)	(K)	(17)	(18)
NGC 266	L1.9	2.0	62.4	39.3	00 49 47.8152	32 16 39.740	3.2	3.8	...	21.17	5.7×3.1	...	> 7.1	0.30	1
NGC 315	L1.9	-4.0	65.8	39.5	<i>a</i>	<i>a</i>	350.0	23.26	30	-49	2.5×1.5	-4	≥ 9.8	0.32	4
NGC 524	T2:	-1.0	32.1	38.6	<i>a</i>	<i>a</i>	0.9	1.5	...	20.05	4.5×2.0	-10	> 6.8	0.16	5,19
NGC 1167	S2	-3.0	65.3	40.2	<i>a</i>	<i>a</i>	4.6	5.9	...	21.37	10	141	4.1×1.7	-10	> 7.6	0.32	3,17
NGC 1275	S1.5	10.0	70.1	41.1	<i>a</i>	<i>a</i>	1810.0	24.03	23	0	1.6×1.2	0	≥ 10.8	0.34	6
NGC 2273	S2	0.5	28.4	40.4	06 50 08.6578	60 50 44.901	2.0	2.4	3.5	20.29	1.5	-90	3.0×1.7	6	≥ 7.4	0.14	3
NGC 2655	S2	0.0	24.4	39.5	<i>a</i>	<i>a</i>	...	< 0.8	...	< 19.73	4.8×4.3	45	> 6.4	0.12	2
NGC 2768	L2	-5.0	23.7	39.0L	09 11 37.4127	60 02 14.859	5.6	7.3	...	20.58	2.7×1.6	-21	> 7.9	0.11	3
NGC 2787	L1.9	-1.0	13.0	38.5	09 19 18.6057	69 12 11.645	11.2	11.5	...	20.36	4.3×1.6	...	> 8.0	0.06	1
NGC 2911	L2	-2.0	42.2	39.8L	09 33 46.1074	10 09 08.819	22.4	29.1	...	21.68	3.4×1.6	3	> 8.4	0.20	3
NGC 3031	S1.5	2.0	3.6	37.6L	<i>a</i>	<i>a</i>	120.0	...	132.0	20.27	0.8	50	0.5×0.5	0	≥ 10.0	0.02	7
NGC 3079	S2	7.0	20.4	38.8	<i>a</i>	<i>a</i>	16.0	18.0	...	20.90	55	125	8.4×2.5	3	≥ 7.7	0.10	8
NGC 3147	S2	4.0	40.9	39.5	10 16 53.6509	73 24 02.695	6.0	8.1	...	21.08	1.6×1.2	27	> 8.3	0.20	2,15
NGC 3169	L2	1.0	19.7	39.0	10 14 15.0503	03 27 57.875	6.2	6.6	...	20.46	4.5×1.7	...	> 7.7	0.10	1
NGC 3226	L1.9	-5.0	23.4	38.9	10 23 27.0083	19 53 54.465	3.5	4.8	...	20.36	...	64	3.9×1.8	...	> 7.5	0.11	1
NGC 3227	S1.5	1.0	20.6	40.4L	<i>a</i>	<i>a</i>	0.8	0.8	...	19.61	0.10	14
NGC 3516	S1.2	-2.0	38.9	40.2L	11 06 47.4634	72 34 07.278	1.8	2.1	...	20.51	3.6×2.6	35	> 7.1	0.19	3,19
NGC 3718	L1.9	1.0	17.0	38.5L	11 32 34.8530	53 04 04.517	3.4	5.3	...	20.07	2.2×1.7	-54	> 7.8	0.08	2
NGC 3998	L1.9	-2.0	21.6	40.0	<i>a</i>	<i>a</i>	78.2	83.0	...	21.64	7.4×4.7	26	> 8.1	0.10	9
NGC 4143	L1.9	-2.0	17.0	38.7	12 09 36.0679	42 32 03.036	8.1	8.7	...	20.45	2.3×1.2	-41	> 8.3	0.08	2
NGC 4151	S1.5	2.0	20.3	41.2L	<i>a</i>	<i>a</i>	2.5	...	10.0	20.09	...	77	2.1×1.8	-67	≥ 8.7	0.10	10
NGC 4168	S1.9:	-5.0	16.8	37.6	12 12 17.2685	13 12 18.701	2.5	2.5	...	19.93	3.2×1.5	10	> 7.5	0.08	2,15
NGC 4203	L1.9	-3.0	9.7	38.3	12 15 05.0554	33 11 50.381	8.9	8.9	...	20.00	3.8×1.6	...	> 8.0	0.05	1,15
NGC 4258	S1.9	4.0	6.8	38.3	<i>a</i>	<i>a</i>	1.7	...	3.0	18.97	0.5	0	1.0×1.0	0	> 6.7	0.03	11,19
NGC 4261	L2	-5.0	35.1	39.3	<i>a</i>	<i>a</i>	80.0	...	390.0	22.07	25	90	2.8×1.1	-5	≥ 9.2	0.17	12
NGC 4278	L1.9	-5.0	9.7	39.2	12 20 06.8254	29 16 50.715	37.3	...	65.2	20.62	10	0	2.5×2.5	0	> 8.6	0.05	1
NGC 4374	L2	-5.0	16.8	38.9	12 25 03.7433	12 53 13.142	160.0	...	186.0	21.73	11	0	2.7×1.4	7	≥ 9.4	0.08	2
NGC 4395	S1.8	9.0	3.6	37.9L	<i>a</i>	<i>a</i>	...	0.5	...	17.91	> 6.3	0.02	18
NGC 4450	L1.9	2.0	16.8	38.9L	<i>a</i>	<i>a</i>	3.6	3.6	...	20.08	0.08	16,19
NGC 4472	S2::	-5.0	16.8	37.6c	12 29 46.7619	08 00 01.713	2.2	2.3	...	19.87	3.4×1.5	5	> 7.4	0.08	2
NGC 4486	L2	-4.0	16.8	39.4	<i>a</i>	<i>a</i>	450.0	22.18	...	290	2.0×0.8	-11	> 10.2	0.08	13
NGC 4552	T2:	-5.0	16.8	38.5	12 35 39.8073	12 33 22.829	99.5	...	139.0	21.53	7.0	80	2.9×1.2	2	> 9.2	0.08	2
NGC 4565	S1.9	3.0	9.7	38.0	12 36 20.7802	25 59 15.629	3.2	3.2	...	19.56	3.8×1.6	...	> 7.5	0.05	1
NGC 4579	S1.9/L1.9	3.0	16.8	39.4	12 37 43.5222	11 49 05.488	21.0	21.0	...	20.85	4.2×1.5	...	> 8.3	0.08	1,15
NGC 4589	L2	-5.0	30.0	39.1	12 37 24.9865	74 11 30.889	6.0	8.1	11.5	20.81	4.5	118	2.1×1.5	-15	> 8.1	0.15	3
NGC 4772	L1.9	1.0	16.3	38.5L	12 53 29.1613	02 10 06.157	1.8	1.8	...	19.76	5.0×4.0	0	> 6.8	0.08	2
NGC 5322	L2::	-5.0	31.6	38.8b	13 49 15.2653	60 11 25.929	10.8	12.0	...	21.11	2.8×1.4	-2	> 8.2	0.15	3
NGC 5353	L2/T2:	-2.0	37.8	39.1	13 53 26.6945	40 16 58.877	13.1	20.4	21.6	21.35	3.5	68	2.9×2.2	36	> 8.1	0.18	3
NGC 5354	T2/L2:	-2.0	32.8	38.7	<i>a</i>	<i>a</i>	2.4	6.6	8.6	20.49	4.0	90	2.3×1.6	7	≥ 7.6	0.16	5
NGC 5363	L2	10.0	22.4	39.4	13 56 07.2141	05 15 17.264	25.5	30.4	39.6	21.19	6.7	-100	3.6×1.4	-7	≥ 8.5	0.11	3
NGC 5846	T2:	-5.0	28.5	38.8	<i>a</i>	<i>a</i>	0.6	1.1	2.4	19.77	11	0	3.4×1.4	-1	≥ 6.9	0.14	5
NGC 5866	T2	-1.0	15.3	38.0	15 06 29.4988	55 45 47.568	7.0	8.4	...	20.29	...	11	3.9×1.4	...	> 7.9	0.07	1
NGC 6500	L2	1.7	39.7	40.3	17 55 59.7822	18 20 17.668	35.8	...	73.3	21.83	5.0	39	2.5×2.5	0	≥ 8.6	0.19	1
NGC 7626	L2::	-5.0	45.6	38.8	23 20 42.5379	08 13 00.984	18.2	24.1	25.7	21.66	1.5	32	3.9×1.5	-18	≥ 8.3	0.22	3

Note. — This table lists all AGNs and LLAGNs in the Palomar sample which have been imaged with VLBI techniques. Unless otherwise noted in the references cited in col. 18 the listed results are for 5 GHz observations with the VLBA or a global-VLBI network.

Columns are: (1) galaxy name; (2) nuclear activity type as explained in Table 1; (3) Hubble morphological parameter T as listed in H97a; (4) distance in Mpc to galaxy, as listed in H97a; (5) Log of the H α luminosity as listed in H97a. The flags (also from H97a) denote the following: *L* non-photometric data, *b* 50% uncertainty, *c* 100% uncertainty; (6) and (7) VLBA 5 GHz radio position listed for sources observed by our group - these positions have been updated to reflect the most recently available accurate positions for the phase-reference sources. For other sources (marked with an ^a), col. 18 lists the appropriate reference; (8) and (9) peak and total flux-density, obtained by fitting a single Gaussian to the nuclear source; (10) total mas-scale flux in the VLBI maps; (11) logarithm of the nuclear radio luminosity (derived from the *peak* radio flux); (12) and (13) extent and position angle (deconvolved from the beam) of the mas-scale radio emission; (14) and (15) beam size and beam position angle of the maps from which the previous columns data are derived; (16) implied brightness temperature of the nucleus; (17) linear scale on sky (parsec per milliarcsec); and (18) Comments as listed below.

Comments: 1. data from Falcke et al. 2000 (radio positions updated here); 2. data from Nagar et al. 2002 (radio positions updated here); 3. new data from this paper; 4. data from Cotton et al. (1999); 5. data from Filho et al. (2003); 6. data from Walker et al. (2000); 7. 8.4 GHz data from Bietenholz et al. (2001); 8. data from Trotter et al. (1998); 9. data from Filho et al. (2002); 10. 1.4 GHz VLBI data from Mundell et al. (2003); 11. data from Herrnstein et al. (1997); 12. data from Jones et al. (2001); 13. data from Junor et al. (1999); 14. data from J. Gallimore, priv. communication; 15. see also Anderson et al. (2004); 16. data from Anderson et al. (2004); 17. mas-scale extent and P.A. from Giovannini et al. (2001); 18. 1.4 GHz data from Wrobel et al. (2001); 19. S_{15 GHz}^{VLA} < 2.7 mJy in Table 1.